# Chapter 11

# Remote Sensing of Vegetation: Potentials, Limitations, Developments and Applications

Mathias Disney*
*Department of Geography, University College London, Gower Street, London WC1E 6BT, UK*

*NERC National Centre for Earth Observation*



## Summary

Earth observation, i.e., gaining information of Earth's physical, chemical and biological characteristics by remote sensing methods, can be used to make a range of quantitative measurements related to vegetation canopy structure and function. The capabilities of Earth observation for mapping, even indirectly, canopy state and function over wide areas and over decadal time-scales allow for studies of phenology, disturbance, anthropogenic impacts and

*Author for correspondence, e-mail: mathias.disney@ucl.ac.uk

K. Hikosaka, Ü. Niinemets, and N.P.R. Anten (eds.), *Canopy Photosynthesis: From Basics to Applications*, DOI 10.1007/978-94-017-7291-4_11

responses to climate change. Key limitations of Earth observation measurements are discussed, in particular how their indirect nature makes them potentially hard to interpret and relate to physically-measurable quantities, as well as assumptions that are made to derive information from Earth observation data. Various Earth observation measurements of vegetation routinely provided from satellite data are introduced and a radiative transfer framework for developing, understanding and exploiting these measurements is outlined. This framework is critical in that it allow us to chart a consistent route from measurements made at the top-of-the atmosphere to estimates of canopy state and function. The impacts of assumptions required to solve the canopy radiative transfer problem in practical applications are discussed. New developments in radiative transfer theory and modelling are introduced, in particular focusing on how incorporating the vegetation structure in these models is key to interpreting many Earth observation measurements. These new techniques help to unpick the nature of the canopy signal from Earth observation measurements. The (key) issue of 'effective' model parameters that are often used to interpret and exploit observations is raised. These simplified or approximate manifestations of measurable physical properties permit development of practical, rapid models of the sort required for global applications but potentially introduce inconsistency between Earth observation measurements and models of vegetation productivity. Methods to overcome these limitations are discussed, such as data assimilation, which is being used to provide consistent model-data frameworks and make best use of both. Lastly, new remote sensing measurements are described that are providing information on 3D

*Abbreviations*: $A_l$ – Area of a given leaf; ALS – Airborne laser scanning; BRDF – Bidirectional reflectance distribution function; c – Speed of light; d – Sensor-target distance; DA – Data assimilation; DASF – Directional area scattering factor; DEM – Digital elevation model; DGVM – Dynamic global vegetation model; DWEL – Dual-wavelength Echidna laser scanner; $E_i$ – Downwelling surface irradiance; EO – Earth observation; ESA – European Space Agency; ESM – Earth system model; ESS – Earth system science; EVI – Enhanced vegetation index; fAPAR – Fraction of absorbed photosynthetically active radiation; $F_s$ – Solar-induced chlorophyll fluorescence; FTS – Fourier Transform Spectrometer; $g_l(z, \mathbf{\Omega}_l)$ – Angular distribution of leaf normal vectors (leaf angle distribution); $G_l(\mathbf{\Omega})$, $G_l(\mathbf{\Omega}')$ – Leaf projection function in direction $\mathbf{\Omega}$, $\mathbf{\Omega}'$ respectively; GLAS – Geoscience Laser Altimeter System; GO – Geometric optics; GOSAT – Greenhouse Gases Observing Satellite; GPP – Gross primary productivity; $h_l(\phi_l)$ – Azimuthal dependence of leaf angle, $\phi_l$; $H$ – Canopy total height; $H(\boldsymbol{x})$ – Observation operator, mapping model state variable vector $\boldsymbol{x}$ to the EO signal; $i_0$ – Radiation first intercepted in the canopy by leaves; $i_L$ – Leaf interceptance that enters the leaf interior; $I_r$ – Upwelling (reflected) radiance; $I(z, \mathbf{\Omega})$ – Specific energy intensity in direction $\mathbf{\Omega}$ at depth $z$ in a horizontal plane-parallel canopy; $J_s(z, \mathbf{\Omega}')$ – Source term of radiative transfer equation at depth z, in direction $\mathbf{\Omega}'$; $\kappa_e$ – Volume extinction coefficient; $L(z)$ – Cumulative leaf area index at depth $z$; LAD – Leaf angle distribution; LAI – Leaf area index; $L\tilde{A}I$ – Effective LAI; lidar – Light detection and ranging; LSM – Land surface model; MCRT – Monte Carlo ray tracing; MERIS – Medium Resolution Imaging Spectrometer; MISR – Multiangle Imaging Spectroradiometer; MODIS – Moderate Resolution Imaging Spectroradiometer; $N_v(z)$ – Number of leaves per unit volume; NASA – National Aeronautics and Space Administration; NDVI – Normalized difference vegetation index; NIR – Near infrared; NPP – Net primary productivity; $p$ – Recollision probability; $P\left(z, \mathbf{\Omega}' \rightarrow \mathbf{\Omega}\right)$ – Volume scattering phase function; PFT – Plant functional type; PILPS – Project for Intercomparison of Land Surface Parameterization Schemes; $Q_0$ – Uncollided radiation passing through the canopy to the lower boundary layer; $\boldsymbol{R}$ – Vector of EO measurements; RADAR – Radio detection and ranging; RAMI – Radiation Transfer Model Intercomparison; $\boldsymbol{S}$ – Radiation model system state vector; SALCA – Salford Advanced Laser Canopy Analyser; SWIR – Shortwave infrared; t – Time of flight; TANSO – Thermal and Near infrared Sensor for carbon Observation; TLS – Terrestrial laser scanning; $z$ – Canopy depth; $\boldsymbol{Z}$ – Radiation signal modelled by a radiation model with state variable $\boldsymbol{S}$; $W_\lambda$ – Spectral canopy scattering coefficient; $\zeta$ – Canopy clumping factor; $\lambda$ – Wavelength; $\mu$, $\mu'$ – Cosine of the view, illumination direction vectors $\mathbf{\Omega}$, $\mathbf{\Omega}'$ with the local normal; $\rho$ – Reflectance; $\tau$ – Transmittance; $\theta_{v,i}$ – View, illumination zenith angles; $\varphi_{v,i}$ – View, illumination azimuth angles; $u_l(z)$ – Canopy leaf area density at depth $z$; $\omega$ – Leaf single scattering albedo; $\hat{\omega}_\lambda$ – Spectral leaf single scattering albedo normalized by leaf interceptance; $\mathbf{\Omega}(\theta_v, \varphi_v)$ and $\mathbf{\Omega}'(\theta_i, \varphi_i)$ – View, illumination vectors

canopy structure, from lidar particularly, and canopy function from fluorescence. These measurements, along with other Earth observation data and model-data fusion techniques are providing new insights into canopy state and function on global scales.

## I. Introduction

### *A. What Is Earth Observation?*

Terrestrial vegetation is a key component of the Earth's climate system, via mediation of fluxes of solar radiation, water and atmospheric gases at the land surface, and the resulting interactions with and feedback to the global carbon cycle (Denman et al. 2007; Solomon et al. 2007). Terrestrial vegetation processes operate across a huge range of time-scales, responding from seconds to hourly and daily time-scales to changes in environmental conditions temperature, precipitation and light, and over seasonal and much longer time-scales to cycles of climate and global change. Vegetation is also heterogeneous at a huge range of scales (within leaf, root systems) to composition of savannahs and forests shaped by millennia of evolutionary, climate and more recently anthropogenic influences. Vegetation is of course also intimately connected to human activity in provision of food, shelter, fuel and many other direct and indirect ecosystem services.

The importance of understanding the state and function of vegetation has led to development of a wide range of observational and modelling techniques (Sellers 1985; Liang 2004; Monteith and Unsworth 2008; Jones 2014). Of these, remote sensing (hereafter referred to as Earth observation (EO), to distinguish it from planetary remote sensing) has become a central part of efforts to address many of these issues due to the large spatio-temporal scales that can be covered by satellite and airborne instruments. The developments of EO have seen huge advances in instrument design, accuracy, consistency and the ability to handle large (and ever-growing) datasets (Lynch 2008). These benefits have led to EO becoming ubiquitous in Earth System Science. A wide range of problems at global and regional scales are ideally-suited to the scale and coverage of EO. New observations and models have arisen in tandem, sometimes by design, although more often not. This has led to many new developments for exploiting EO data in understanding and measuring the Earth System (Chapin et al. 2011). This has also raised fundamental questions about how such observations can be used (Pfeifer et al. 2012).

Here, I introduce the problem of how EO is used for understanding and quantifying terrestrial vegetation i.e. what can and can't be measured via EO. A key advantage of remote sensing, its remoteness, is also a key limitation: what we actually *can* measure is rarely what we *want* to measure. To translate the former to the latter, a hierarchy of models has been developed. I outline some of the issues and approaches to modelling across this hierarchy: from scattering and absorption of radiation (EO models), through models that transform radiation into canopy properties (state, productivity, dynamics) and on to large-scale models of ecosystem processes, both of the current state (diagnostic, biogeochemical cycling) and future changes (prognostic, dynamic global vegetation models (DGVMs), and their big brothers, global climate models). If and when these various models interface with EO data, they do so in very different ways due to their underlying assumptions, structure and aims. I discuss some of the consequences of these variations (and inconsistencies) from the point of view of how EO can be used to understand and quantify terrestrial vegetation systems, as well as how models may be developed to better exploit EO data. Clearly, quantifying the state of terrestrial ecosystems and understanding how they will change in the face of uncertain climate and anthropogenic drivers, requires best use of both observations and models.

### *B. What Earth Observation Can and Can't Measure*

The value of an EO measurement is simply the answer to the question: how much

information about the system being observed is contained within the EO measurement of that system? The EO signal is a measure of scattered (reflected, transmitted) or emitted radiation from a target. We measure photons escaping towards a sensor, from a target, either above the atmosphere in the case of a satellite, or at some point lower down in the case of airborne or even ground-based observations. Table 11.1 describes a list of properties that EO can and does provide, along with an assessment of the level of how 'direct' these measurements are in some sense, from the perspective of any additional ground-level measurements or modelling needed to interpret the measurements. Not surprisingly, as EO 'measurements' become less direct, three critical (and related) things occur:

- The number of assumptions underlying an EO measurement becomes larger and the opportunity for these assumptions to become inconsistent at some level increases.
- The uncertainty associated with an EO measurement becomes more difficult to quantify (albeit not necessarily larger), due to the increasing number of assumptions and requirements for ancillary information, and the way uncertainties in each may combine in potentially non-linear ways.
- The more difficult it is likely to be to compare an EO measurement against independent measurements (or model-derived estimates) of what ought to be the same property. This is due to possible differences in underpinning assumptions and ancillary information.

These issues of the limits of remote sensing measurement are identified by Verstraete et al. (1996). They define a physical model relationship between an observation of emitted radiation $\boldsymbol{Z}$ and a system described by model state variables $\boldsymbol{S}$ as

$$\boldsymbol{Z} = f\boldsymbol{S} \tag{11.1}$$

where the $\boldsymbol{S}$ are the smallest set of variables needed to fully describe the physical state of the observed system, at the scale of observation. It is worth repeating the first proposition of Verstraete et al. (1996) on the limitations of remote sensing, as it provides a useful framing for the ensuing discussion: "A physical interpretation of electromagnetic measurements $\boldsymbol{Z}$ obtained from remote sensing can provide reliable quantitative information *only on the radiative state variables* $\boldsymbol{S}$ *that control the emission of radiation from its source and its interaction with all intervening media and the detector*" (emphasis added). We may be able to translate from $\boldsymbol{S}$ to other parameters of interest that may rely on $\boldsymbol{S}$ indirectly (e.g. canopy state or function), but we always require a mapping back to $\boldsymbol{S}$ at some point if we wish to make use of remote sensing.

The last category in Table 11.1 is intended to indicate properties that are either not well-defined (i.e. do not have a clear physically-derived meaning), or perhaps are not directly measurable quantities i.e. in the formalism of Verstraete et al. (1996) we are not able to define a physically-based mapping $\boldsymbol{Z} = f(\boldsymbol{S})$ for these parameters. However, such properties may be used to capture some aspect of the canopy either for (empirical) correlation with some more desirable variable, or for parameterizing more complex models. Examples include vegetation indices such as the normalized difference vegetation index (NDVI) and variants, which have been widely and successfully used to provide surrogate indicators of canopy 'greenness' (Pettorelli et al. 2005). They are attractive due to being easy to calculate and apply, and they may capture key aspects of vegetation 'well enough'. NDVI for example exploits the characteristic high contrast between red and near-infrared (NIR) spectral reflectance, $\rho$ of healthy vegetation as $\mathrm{NDVI} = (\rho_{NIR} - \rho_{RED})/(\rho_{NIR} + \rho_{RED})$. Such indices are clearly useful for capturing particular broad vegetation patterns, in themselves e.g. as indicators of vegetation response to climate, disturbance, insect or fire damage, malaria risk etc. (Pettorelli et al. 2005, Pettorelli 2013; Pfeifer et al. 2012). Vegetation indices can also be used as surrogates for empirically-related variables such as leaf area index (LAI), the (unitless) one sided leaf area per unit

*Table 11.1.* List of properties of interest to terrestrial ecosystem studies that can be derived from EO data, categorised broadly by their requirement for additional information and assumptions beyond a direct measurement

| 'Directness' | Measurement (units) | Key additional assumptions |
|---|---|---|
| Direct | Top-of-atmosphere at-sensor radiance (W $m^{-2}$ $sr^{-1}$ $\mu m^{-1}$) from reflectance (optical), emittance (passive microwave/thermal), backscatter (RADAR); canopy fluorescence (arbitrary units). | Calibrated sensor response, geolocated instantaneous field of view (IFOV) |
| | Distance from sensor to target i.e. canopy and surface height (m) e.g. from lidar | Accurate time-of-flight of active (generated) signal (pulse), known pulse characteristics and position of sensor in 3D space. |
| High | Top-of-canopy (surface) radiance (W $m^{-2}$ $sr^{-1}$ $\mu m^{-1}$) | Known atmospheric path radiance (via models and/or ancillary data) |
| | Albedo (unitless) | Known incoming radiation distribution in terms of angular and direct-to-diffuse ratio i.e. function of atmosphere; integrable model of surface angular reflectance distribution |
| | Surface temperature (K) | Well-calibrated sensor; surface emissivity |
| Medium | Canopy structural properties: Leaf area index (LAI, unitless); canopy cover (unitless %); canopy gap fraction (unitless) | Model relating scattered radiation to structural parameters, assume a degree of clumping/ Inversion must be tractable and not ill-posed. |
| | Canopy radiometric properties: fraction of photosynthetically active radiation, fAPAR (unitless); canopy-average biochemical constituents (chlorophyll, water, N and dry matter, mass per unit specific leaf area i.e. g $m^{-2}$) | Model relating radiation scattered within and from the canopy to radiometric parameter. Inversion must be tractable and not ill-posed. |
| | Leaf radiometric properties: biochemical constituents (chlorophyll, water, N and dry matter, mass per unit specific leaf area i.e. g $m^{-2}$) | Model relating radiation scattered within and from the leaf. Often embedded into canopy-level model. |
| | Standing biomass (kg C $m^{-2}$) | Empirical allometric model relating height to biomass (via time-of-flight from lidar, or interferometric RADAR); requires woody biomass to total carbon ratio. |
| | Fire radiative power (FRP, W $m^{-2}$ $\mu m^{-1}$) and energy (FRE) (J $m^{-2}$) | FRP requires model relating observed temperature to surface emissivity; FRE requires integration of FRE over time. |
| | Burned area (ha) | Model of surface bidirectional reflectance distribution function (BRDF) allowing prediction of reflectance and detection of change. |
| Low | Standing biomass (kg C $m^{-2}$) from scattering | Model of reflectance (optical) or backscatter (RADAR) related to biomass; assumption of leaf to wood ratio in canopy and wood density conversion factor; |
| | Photosynthetic rate ($\mu$mol $m^{-2}$ $s^{-1}$) | Model relating leaf absorption or fluorescence, to measured signal |
| | Gross primary productivity, GPP (kg C $m^{-2}$ $h^{-1}$) | Incoming radiation, fAPAR, model relating intercepted radiation to gross productivity; ancillary information on biome type, climate (T, P) |
| | Net primary productivity, NPP (kg C $m^{-2}$ $h^{-1}$) | GPP, autotrophic respiration losses (measured or modelled) |
| | Net ecosystem productivity, NEP (kg C $m^{-2}$ $h^{-1}$) | NPP, heterotrophic respiration losses (measured or modelled) |

(continued)

*Table 11.1.* (continued)

| 'Directness' | Measurement (units) | Key additional assumptions |
|---|---|---|
| | Net ecosystem exchange, NEE (kg C $m^{-2}$ $h^{-1}$) | NEP, losses due to disturbance (fire, harvest, predation, etc) |
| | Land cover ($km^{-2}$), Land use/land use change (LULUC, $km^{-2}$) | Unique mapping of vegetation types (or biome) and other spectrally identifiable cover types to land cover classes; LULUC requires mapping between biome/land cover and land use. |
| Ambiguous/ surrogate | NDVI (and other empirical spectral indices); 'greenness'; phenology. | Land cover or biome type; spectral; definition of 'greenness' – usually some arbitrary translation of a spectral index to vegetation 'vigour' or state; phenology requires definition of canopy timing, as a function of an EO-derived variable, typically NDVI or LAI. |

Key assumptions required to move from more to less direct measurements are outlined. The list is not intended to be exhaustive, and 'directness' is somewhat subjective.

ground area, fraction of absorbed photosynthetically active radiation (fAPAR) and hence productivity (Myneni and Williams 1994; Myneni et al. 1997a; Angert et al. 2005). However, simplicity comes at the cost of ecological meaning (i.e. direct causality) and requirement for site- or biome-specific calibration (e.g. Nagai et al. 2010). Other more general limitations of vegetation indices are the lack of sensitivity with increasing LAI, saturating at values of 4–5, and sensitivity to background effects (soil, haze etc.). Care is also needed when compositing vegetation indices over time to account for variations in view and sun angles in the reflectance observations from which the vegetation indices are derived. These limitations, particularly saturation, are not soluble through taking a particular calibration approach.

The difficulty of interpreting vegetation indices has been seen in the debate over unexpected trends in Amazonian green-up observed during the severe 2005 drought (Saleska et al. 2007; Samanta et al. 2010). Subsequent to this, work relating carefully re-processed estimates of enhanced vegetation index (EVI, another empirical spectral index) to ground-based measures of productivity, water availability and other ecological variables suggested that apparent discrepancies may be due to leaf flushing being mistaken for changes in LAI and productivity (Brando et al. 2010). This debate was rejoined by recent re-analysis of the satellite data, including detailed consideration of vegetation structure and satellite-sun geometry (Morton et al. 2014). This approach accounts for the apparent 'observed' green-up, whilst also ruling out the leaf-flushing hypothesis. Crucially, this re-analysis was carried out on the original satellite spectral reflectance data, rather than the spectral indices derived from those data from which the original 2005 green-up conclusions were drawn.

This debate perhaps illustrates the difficulty of trying to explain variations in empirical spectral indices that can be functions of complex, often mutually compensating biophysical processes. Verstraete et al. (1996) sum up this difficulty by noting that any number of empirical functions relating a parameter of interest $\boldsymbol{Y}$ to observations $\boldsymbol{Z}$ of the form $\boldsymbol{Y} = g(\boldsymbol{Z})$ may be derived. However, these relationships effectively assume that the variable of interest is the main controlling factor of the observations $\boldsymbol{Z}$ to the (near) exclusion of all other factors. Since the same vegetation index is often used to derive different $g(\boldsymbol{Z})$ for different applications, the information contained in $g(\boldsymbol{Z})$ must be the same, regardless of how the vegetation index is interpreted. This is rarely acknowledged in practice.

The problem of ascribing direct meaning to surrogate variables makes them hard (or even impossible) to validate. For example 'greenness' has been used to imply amount (Myneni et al. 1997a), productivity, health (degree of stress) and phenology (Myneni et al. 2007; Pettorelli 2013). This latter

term is also ambiguous; although it implies seasonality, this can be defined to encapsulate a number of different, related things: bud break, leaf emergence, onset of photosynthesis and growth, start of flowering, seasonal LAI profile, onset of senescence, leaf drop, growing season length etc. A further complication is that ecological models that describe plant seasonality typically use some integrated estimate of time such as growing degree days (number of days over a base threshold, $T_t$ multiplied by the excess temperature $T$-$T_t$). Recent work by Richardson et al. (2012) has shown that different model representations of phenology tend to introduce overestimates of canopy productivity during spring greenup by 13 %, and during autumn senescence by 8 % of total annual productivity. This problem was exacerbated by the tendency of individual models to compensate for over-estimates during transition periods by under-prediction of summer peak productivity. As a result, Richardson et al. (2012) conclude that current model uncertainties preclude reliable prediction of future phenological response to climate change.

The difference between the ways ecological models treat vegetation amount and state and how these properties can be derived from EO is a key reason for differences between models and observations: both representations may be internally consistent, but inconsistent with each other (of course, either or both may be wrong as well!). Lastly, even when empirically-derived properties appear to correlate well with characteristics we wish to measure, we do not know how the residual unexplained variance arises, or if it is important. For a more detailed discussion I refer to Pfeifer et al. (2012) and Grace et al. (2007) who review a range of ecologically-relevant biophysical properties available from EO, as well as some of the issues in moving from direct to more indirect products.

Perhaps most importantly then, for understanding and interpreting EO-derived measurements of canopy state and function, we require physically-based models of radiation interaction with the canopy. Below, I provide a statement of this problem, lay out some of approaches to solving it, and describe how these approaches are used to exploit the EO signal for remote sensing studies of vegetation. Advances in computing power have meant that highly-detailed modelling approaches which were previously impractical have become increasingly attractive. A good example of this is how photo-realistic 3D modelling techniques developed by the computer graphics community for movie-making and visualisation, have been co-opted for modelling vegetation for scientific applications (Disney et al. 2006; Widlowski et al. 2006). This in turn has led to improved parameter estimation schemes (Disney et al. 2011), allowed assessed of uncertainty, and provided test and benchmark tools for simpler modelling approaches (Widlowski et al. 2008, 2013). Rapid increases in computation speed have also led to changes in the way information can be derived from very large (GB to TBs) satellite datasets. This is almost always a balance between requirements for speed/efficiency, and accuracy or physical realism. Increasingly, statistical tools such as Monte Carlo and Bayesian methods, which had been too slow for these applications, can be employed (Sivia and Skilling 2006).

I discuss some of these developments in canopy modelling in more detail below, before moving on to discussing recent developments in model-data fusion that are pushing the limitations of both, and the advent of new observations that may provide information more directly-related to the problems at hand. I embark on this description with a quote that encapsulates the difficulty that can arise in trying to reconcile models (hypotheses) and measurements, in part due to the different scientific drivers and assumptions that underlie them; this is particularly apposite in remote sensing, where the two are so intimately intertwined.

> A hypothesis is clear, desirable and positive, but is believed by no one but the person who created it. Experimental findings, on the other hand, are messy, inexact things which are already believed by everyone except the person who did the work (Harlow Shapley (1885–1972), *Through Rugged Ways to the Stars*, 1969).

## II. Radiative Transfer in Vegetation: The Problem and Some Solutions

We are rarely interested in the most direct EO measurement we can make i.e. in top-of-atmosphere radiance resulting from photons incident on the surface that are scattered in some way back towards the sensor (Pfeifer et al. 2012). In order to relate the above-atmospheric signal to the structural (amount, arrangement) and biochemical (absorbing species and concentrations) properties of the canopy we need a physically-realistic description of the radiation scattering properties of the canopy. This in turn requires understanding of the canopy radiative transfer (RT) regime from the leaf level, across scales to shoot and crown levels, and finally to the whole canopy.

### *A. Statement of the Radiative Transfer Problem*

RT models have been used extensively since the 1960s to model scattering from canopies at optical wavelengths (Ross 1981; Myneni et al. 1989). The models consider energy balance across an elemental volume in terms of the energy arriving into the volume (either energy incident in the propagation direction, or energy that is scattered from other directions) and energy losses from the volume (either scattering out of the propagation direction, or absorption losses). Across optical wavelengths (visible, NIR and shortwave infrared (SWIR) regions of 400–2500 nm) a scalar radiative transfer equation is used. At RADAR wavelengths (cm to m), a slightly different approach is required, incorporating a vector of intensities to allow consideration of polarization (controlled by the sensor design). In this case orthogonal polarizations are coupled so radiative transfer equations must take this into account in a vector solution. Here I focus on radiative transfer in the optical domain, due to the particular relevance to canopy activity.

A widely-applied approach to describing radiation transport in vegetation has been via the so-called turbid medium approximation (Ross 1981; Myneni et al. 1989; Liang 2004). This considers the canopy as a plane parallel homogeneous medium of infinitesimal, oriented scattering elements, suspended over a scattering (soil) background – a 'green gas'. In this case, mutual shading can be ignored (the 'far field' approximation) and the radiance field resulting from single and multiple scattered photons can be described by considering the conservation of energy within a canopy layer, and specifying the sources of radiation external to that layer (boundary conditions). The result is an integro-differential equation describing the change in intensity I along a viewing direction $\mathbf{\Omega}(\theta_v, \varphi_v)$ due to: (i) interactions causing radiation to be scattered out of the illumination direction $\mathbf{\Omega}'(\theta_i, \varphi_i)$ (sink term); and (ii) interactions causing radiation to be scattered from other directions into the viewing direction $\mathbf{\Omega}(\theta_v, \varphi_v)$ (source term), where $\theta_{i,v}$ and $\varphi_{i,v}$ are the illumination and view zenith and azimuth angles respectively. This system is shown schematically in Fig. 11.1.

The far-field approximation allows us to ignore polarization, frequency shifting interactions and emission, in which case the upward and downward energy fluxes within the canopy are described by the (1D) scalar radiative transfer equation. For a plane parallel medium (air) embedded with a low density of small scattering objects the radiative transfer equation is composed of two terms, the (negative) extinction term with depth z that is determined by the path length through the canopy and the extinction along this path, and the source term due to multiple scattering from all directions within an elemental volume in the canopy into direction $\mathbf{\Omega}$ by the objects in the volume. Thus,

$$\mu \frac{\partial I(z,\mathbf{\Omega})}{\partial z} = -\kappa_e I(z,\mathbf{\Omega}) + J_s\left(z,\mathbf{\Omega}'\right) \quad (11.2)$$

where $\partial I(z,\mathbf{\Omega})/\partial z$ is the steady-state radiance distribution function and $\mu$ is the cosine of the (illumination) direction vector $\mathbf{\Omega}'$ with the local normal i.e. the viewing zenith

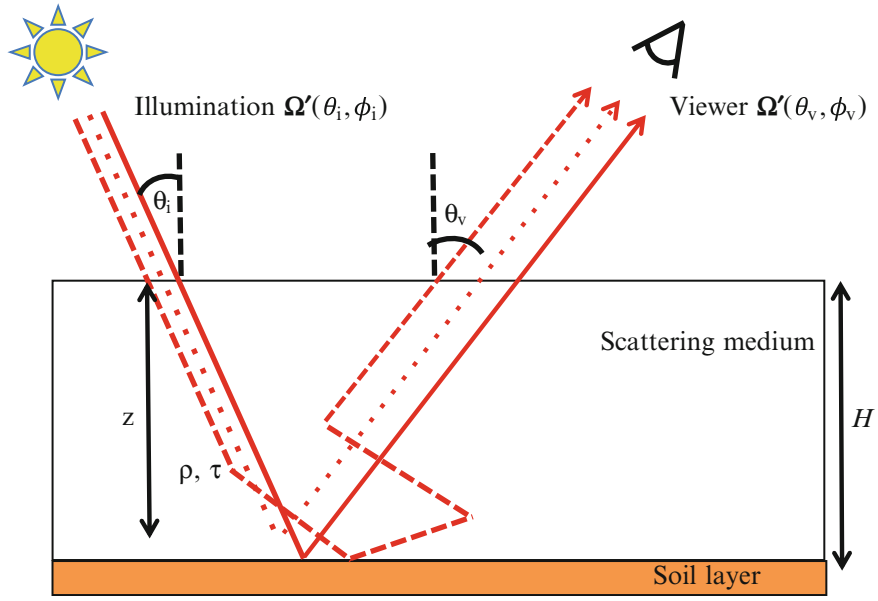


*Fig. 11.1.* Schematic illustration of radiation incident on a plane parallel homogeneous medium (*solid line*), at a zenith angle $\theta_i$ azimuth angle $\phi_i$ from the surface normal and penetrating to a depth $z$ (marked by *dashed line*). In this example incoming radiation either passes through uncollided to the lower boundary, and back up (*solid line*); is scattered once at depth $z$ by reflectance (*dotted line*); or is scattered multiple times via reflectance and/or transmittance, including the canopy lower boundary (at $z = -H$) before escaping in the viewing direction (*dashed line*)

angle, $\theta_i$ used to account for path length through the canopy. The extinction term is given as the product of $\kappa_e$, the volume extinction coefficient, and $I(z, \mathbf{\Omega})$, the specific energy intensity in direction $\mathbf{\Omega}$ at depth $z$ within a horizontal plane-parallel canopy of total height $H$ ($0 < z < H$). The source term, $J_s(z, \mathbf{\Omega}')$, is defined as

$$J_s\left(z, \mathbf{\Omega}'\right) = \int_{4\pi} P\left(z, \mathbf{\Omega}' \rightarrow \mathbf{\Omega}\right) I\left(z, \mathbf{\Omega}'\right) d\mathbf{\Omega}' \tag{11.3}$$

where $P\left(z, \mathbf{\Omega}' \rightarrow \mathbf{\Omega}\right)$ is the volume scattering phase function. This defines the (angular) probability of a photon at depth z in the canopy being scattered from the illumination direction $\mathbf{\Omega}'$ through a solid angle $d\mathbf{\Omega}'$ into to the viewing direction, $\mathbf{\Omega}$, integrated over the unit viewing hemisphere. This term depends on the size and orientation of scatterers within the canopy (see below).

When this description is extended to 3D, i.e. the canopy can vary in density in vertical and horizontal directions, the illumination and viewing vectors are functions of both the zenith and azimuth angles $\theta_{i,v}$ and $\varphi_{i,v}$ i.e. $\mathbf{\Omega}'(\theta_i, \varphi_i)$ and $\mathbf{\Omega}(\theta_v, \varphi_v)$ respectively.

A full description of radiative transfer should include the corresponding emission source term $J_s(z, \mathbf{\Omega}')$ for wavelengths where this might be significant e.g. for passive microwave (thermal) emissions from objects at ~300 K (~8–20 μm). In this case each object within the medium may need to be considered as an emission source in its own right. However, for optical and RADAR wavelengths, the emission source term is effectively zero.

Solving Eq. 11.2 requires defining $\kappa_e$ in terms of canopy biophysical properties, and considering a particular viewing direction $\mathbf{\Omega}'$, for given boundary conditions. In using Eq. 11.2 to model canopy scattering for remote sensing applications, we wish to phrase the scattered radiation as an intrinsic

property of the canopy, rather than as a function of incident intensity. This permits comparison of measurements made under differing illumination intensities. At optical wavelengths this fundamental intrinsic scattering quantity wavelengths is known as the Bidirectional Reflectance Distribution Function (BRDF) i.e.:

$$\mathrm{BRDF}(\boldsymbol{\Omega},\, p, \boldsymbol{\Omega}',\, p';\lambda) = \frac{dI_{\mathrm{r}}(\boldsymbol{\Omega},\, p', F;\lambda)}{dE_{\mathrm{i}}\left(\boldsymbol{\Omega}',\, p;\lambda\right)} \tag{11.4}$$

where $p$ and $p'$ are the polarization of the received/transmitted wave; $E_{\mathrm{i}}$ is the downwelling irradiance on the surface (W m$^{-2}$); and $I_r$ is the upwelling (reflected) radiance (W m$^{-2}$ sr$^{-1}$). The BRDF of an ideal diffuse (Lambertian) surface is $1/\pi$ (for an unpolarized reflector) and is independent of viewing and illumination angles. As defined, BRDF is an infinitesimal quantity (with respect to solid angle and wavelength), so although it can be modelled, it is not a measurable quantity in this form. In practice, we consider the Bidirectional Reflectance Factor (BRF) $\rho_{\mathrm{c}}(\boldsymbol{\Omega}, \boldsymbol{\Omega}')$, defined as the ratio of radiance leaving the surface around viewing direction $\boldsymbol{\Omega}$, $I(\boldsymbol{\Omega})$ due to irradiance $E(\boldsymbol{\Omega}')$, to the radiance on a flat totally reflective Lambertian surface under the same illumination conditions i.e.

$$\begin{aligned}\rho_{\mathrm{c}}\left(\boldsymbol{\Omega}, \boldsymbol{\Omega}'\right) &= \frac{E\left(\boldsymbol{\Omega}'\right)\mathrm{BRDF}\left(\boldsymbol{\Omega}, \boldsymbol{\Omega}'\right)}{E\left(\boldsymbol{\Omega}'\right)(1/\pi)} \\ &= \pi \mathrm{BRDF}\left(\boldsymbol{\Omega}, \boldsymbol{\Omega}'\right)\end{aligned} \tag{11.5}$$

for an equivalent infinitesimal solid angle definition. As the BRF is defined as the ratio of two radiances, it is a directly measurable quantity and allows for model predictions to be compared with measurements, albeit over instrument finite solid angles (and of course wavelength intervals). Detailed definitions of reflectance nomenclature are given by Nicodemus et al. (1977) and Schaepman-Strub et al. (2006).

### *B. Solving the Radiative Transfer Problem for Explicit Canopy Structure*

To solve the radiative transfer problem for realistic canopies, we need to consider how vegetation structure can be expressed in terms of the equations above, using assumptions that permit physically realistic solutions. Various solutions for the radiative transfer equation have been developed in a range of subjects including astrophysics, particle physics and neutron transport (Chandrasekhar 1960). Most importantly, once we have a solution of Eq. 11.2, if it can be inverted in terms of the canopy parameters it contains, we can then estimate distributions of these parameters from EO measurements of $\rho_{\mathrm{c}}(\boldsymbol{\Omega}, \boldsymbol{\Omega}')$ in the standard inverse problem sense (Twomey 1977; Verstraete et al. 1996; Tarantola 2005). Forward and inverse approaches to canopy modelling have been reviewed in detail by Asrar (1989), Goel and Thompson (2000) and more recently by Liang (2004), among others, and I provide a brief overview here.

Solving the forward radiative transfer problem either requires empirical parameterisations or physically-based approximations of canopy properties including leaf size, leaf angle distribution and 1D or 3D arrangement. Some applications do not require a physically-meaningful interpretation of model parameters, only a reasonable prediction of $\rho_{\mathrm{c}}(\boldsymbol{\Omega}, \boldsymbol{\Omega}')$. For example, many remote sensing applications require comparing observations made over time (and/or using wide-angle sensors). These observations are typically acquired at different view and/or illumination angles, so variations in reflectance caused by these varying view and sun angles (i.e. BRDF effects) must be accounted for, otherwise they may be interpreted as surface changes. A widely-used approach is to fit a simple empirical (or semi-empirical) model of BRDF to observations, and use the resulting (inverted) model parameters to interpolate (or normalize) observations to some fixed view and illumination configuration Dickinson (1983). The simple nature of

semi-empirical BRDF models means they can be inverted rapidly, making them suitable for rapid, large-scale applications. Observations from the NASA MODIS and MISR sensors employ variants of this approach to account for sensor and sun angle variations (Pinty et al. 1989; Wanner et al. 1997).

Physically-based models of BRDF are required to represent three specific processes:

1. Coherent superposition of scattered incident radiation. This is dependent on the mean free path between scattering events within the canopy being of the order of the wavelength of the incident radiation. Coherence is generally ignored for vegetation, but is important for soils.
2. Scattering effects resulting from the arrangement of objects on the surface, i.e. specular reflectance, and reflectance variations caused by geometric-optic shadowing assuming parallel rays of incident radiation.
3. Volume (diffuse) scattering of aggregated canopy elements. This is particularly important for dense vegetation and is modelled using radiative transfer methods as outlined above. As higher orders of photon scattering are considered, the interactions become increasingly random in direction, and the volume scattering component tends to become isotropic.

To solve Eq. 11.2, approximations regarding the leaf scattering properties are often made (e.g. Myneni et al. 1989). Other approaches attempt to include modifications for observed features that occur due to the fact that real vegetation canopies are not turbid media and leaves, branches etc. have finite sizes. The most obvious of these features is the so-called 'hotspot', an increase in reflectance seen when $\mathbf{\Omega}$ and $\mathbf{\Omega}'$ are near-coincident, that arises due to shadowing in the scene being at a minimum (Nilson and Kuusk 1989). An example of this phenomenon is shown in Fig. 11.2 As an example of the importance of considering canopy structure on the EO signal, Morton et al. (2014) demonstrate that the apparent Amazon 'greenup' observed in 2005 can be explained almost entirely as a BRDF effect: most observations made in October in this location are in the hotspot i.e. the observed increase in reflectance is an angular effect.

Perhaps the most difficult problem in solving Eq. 11.2 is that of modelling the source term, $J_s(z, \mathbf{\Omega})$ as this requires keeping a 'scattering history' of each photon from one interaction to the next. This problem is essentially insoluble analytically (Knyazikhin et al. 1992), but numerical approximations can be made or computer simulation models can be used (see below). It is also necessary to define the boundary conditions in the case of a canopy illuminated from above. At the top of the canopy the incident irradiation can be considered as diffuse and direct components of solar irradiation. In addition, some radiation arriving at the base of the canopy re-radiates isotropically back up through the canopy effectively creating a source function at the lower canopy boundary. Modified forms of Eq. 11.2 have been widely used to model canopy reflectance for a range of applications. Further approximations and simplifications have been applied for specific types of canopy, such as row crops or particular tree crown shapes. In these cases, simplifying approximations can be made regarding canopy structure, in particular the vertical and horizontal arrangement of leaves and their angular orientations (distribution functions). Various approaches are summarised by Goel (1988), Strahler (1996), Liang (2004) and Lewis (2007, from http://www2.geog.ucl.ac.uk/~plewis/CEGEG065/rtTheoryPt1v1.pdf and http://www2.geog.ucl.ac.uk/~plewis/CEGEG065/rtTheoryPt2v7-1.pdf).

Separation of canopy fluxes into uncollided and collided intensities of various orders (Kubelka and Munk 1931; Suits 1972; Hapke 1981) has often been employed in order to simplify the radiative transfer approach (Norman et al. 1971; Myneni et al. 1990; Verstraete et al. 1990). The simplest two-stream approach decomposes multiple scattering into total upward and downward diffuse fluxes Meador and Weaver (1980). This can be elaborated in

*Fig. 11.2.* Illustration of the canopy hotspot effect. The image was captured with the sun directly behind the camera (see shadow of aircraft in the centre) and the scene is brightest at the centre, darkening radially outwards due to shadows becoming increasingly visible (author's own, taken over temperate rainforest canopy, Fraser Island, Queensland, Australia)

e.g. a four-stream approximation into fluxes resulting from reflectance and transmittance interactions respectively. The discrete properties of the canopy, those related to the size and distribution of scatterers, tend to impact only the first few orders of scattering and these features tend to become 'smeared out' by higher order multiple scattering interactions. Dividing the radiation field into collided and uncollided intensities as opposed to following a standard radiative transfer treatment may preserve these features.

As the canopy becomes denser, mutual shading of scattering elements cannot be ignored. It also becomes increasingly difficult to justify the use of convenient values for the scattering phase function i.e. the assumptions that leaf normals are randomly oriented and azimuthally invariant in defining leaf normal distribution and leaf projection function. This is clearly partially or wholly violated for a number of canopies, particularly for row-oriented agricultural crops. Various approaches have been proposed to overcome this. However, Knyazikhin et al. (1998) have shown that accounting for the discrete nature of vegetation within a (continuous) radiative transfer description leads to an apparent paradox: the more accurate the representation of canopy geometry, the less accurate the resulting description of radiative transfer and photosynthesis in the canopy is likely to be. This arises because of the discrepancy between the assumption of a continuous homogeneous scattering medium underpinning the radiative transfer approach, and the macroscopic effects of 3D leaf and branch size and distribution. Knyazikhin et al. (1998) point out that the radiative transfer approach assumes that the number of foliage elements in an elementary volume is proportional to this volume (encapsulated in the leaf area density), but the larger leaves become are in relation to the volume, the less this

assumption holds. The impact of this departure therefore decreases as we look at larger scales/volumes.

One of the most powerful approximations used in radiative transfer modelling is to concentrate on single scattering interactions only. These are in many cases the dominant component of canopy scattering (Myneni and Ross 1990), particularly at visible wavelengths. Considering single scattering interactions within a turbid medium, the radiation intensity in the incident direction $\mathbf{\Omega}'$, at a depth z within the canopy can be described using Beer's (Beer-Bouger-Lambert's) Law (Monsi and Saeki 1953) as follows

$$I\left(z,\mathbf{\Omega}'\right) = I\left(0,\mathbf{\Omega}'\right)e^{-\left(\frac{L(z)G\left(\mathbf{\Omega}'\right)}{\mu'}\right)} \tag{11.6}$$

where $I(0, \mathbf{\Omega}')$ is the incident irradiance at the top of the canopy; $L(z)$ is the cumulative leaf area index (LAI) in the canopy at depth $z$ ($m^2$ $m^{-2}$); $G(\mathbf{\Omega}')$ is the leaf projection function i.e. the fraction of leaf area projected in the illumination direction $\mathbf{\Omega}'$; $\mu' = \cos(\theta_i)$.

The exponent in Eq. 11.6 is effectively the extinction coefficient $\kappa_e$ i.e. a measure of the rate of attenuation of radiation in the canopy, and is a function of two things: (i) the amount of material along the path i.e. the domain-averaged optical thickness of the canopy layer $LAI$; and (ii) the volume absorption and scattering properties of the media i.e. loss due to absorption by the particles (leaves) and scattering by the particles away from the direction of propagation (Fung 1994). The term $L(z)$ is better defined as $u_l(z)$, the canopy leaf area density i.e. the vertical distribution of one-sided leaf area per unit canopy volume ($m^2$ of leaf area per $m^3$ of canopy volume). We will see later in Section III that this exponent implicitly encapsulates the fact that canopies are not homogeneous but are actually clumped at multiple scales from leaf to branch to crown. Assuming a constant leaf area of $A_l$, and given a leaf number density of $N_v(z)$ (number of leaves per unit volume, $m^{-3}$), then

$$u_l(z) = N_v(z)A_l \tag{11.7}$$

The integral of $u_l(z)$ over the canopy depth, $H$, gives the LAI i.e.

$$\mathrm{LAI} = \int_{z=0}^{z=H} u_l(z)dz \tag{11.8}$$

In practice, $u_l(z)$ may vary from top to bottom of a canopy, with more material perhaps in the upper parts than in the lower parts. As a result, $L(z)$ can be modelled in various ways in a radiative transfer scheme, but the simplest is to assume it is constant with canopy height $H$ i.e. $u_l = LAI/H$.

The term $G(\mathbf{\Omega}')$ in Eq. 11.6 is the projection of a unit area of foliage on a plane perpendicular to the illumination direction $\mathbf{\Omega}'$. By extension, $G_i(\mathbf{\Omega})$ is the leaf projection function in the viewing direction $\mathbf{\Omega}$, averaged over elements of all orientations and is a (unitless) canopy-average representation of the effective leaf area encountered by a photon travelling in a direction $\mathbf{\Omega}$ within the canopy. $G_i(\mathbf{\Omega})$ is defined as

$$G_i(\mathbf{\Omega}) = \frac{1}{2\pi}\int_{2\pi+} g_i(\mathbf{\Omega}_i)|\mathbf{\Omega}\cdot\mathbf{\Omega}_i|d\mathbf{\Omega}_i \tag{11.9}$$

where $g_i(z, \mathbf{\Omega}_i)$ is the angular distribution of leaf normal vectors, known as the leaf angle distribution (LAD) and is defined so that its integral over the upper hemisphere is 1 i.e.

$$\int_{2\pi+} g(\mathbf{\Omega}_i)d\mathbf{\Omega}_i = 1 \tag{11.10}$$

A wide range of choices for models of $g_i(z, \mathbf{\Omega}_i)$ have been proposed (Ross 1981; Goel and Strebel 1984). A typical assumption is that leaf azimuth angles are independent of azimuth i.e. $g_i(\mathbf{\Omega}_i) = g_i(\theta_i)h_i(\phi_i)$ where $h_i(\phi_i)$ is the azimuthal dependence and can be specified separately as

$(1/2\pi)\int_{\phi_i=0}^{\phi_i=2\pi} h_i(\phi_i)d\phi_i = 1$. If the azimuthal distribution is assumed to be uniform (i.e. random) then $h_i(\phi_i) = 1$ and this allows for expression of $g_i(z, \mathbf{\Omega}_i)$ as a function of $\theta_l$ only and $\int_{\theta_i=0}^{\theta_i=\pi/2} g_i(\theta_i)sin\,\theta_i d\theta_i = 1$. While these assumptions make the formulation of $g_i(\theta_i)$ easier, it is known that many canopies depart from them particularly in the case of strongly-row oriented canopies (crops), or due to environmental factors such as wind and water stress (e.g. wilting) and heliotropism. Tree crowns may also have particular azimuthal arrangement due to branching structure, particularly in conifers. Jones and Vaughan (2010) discuss measured LADs and their departures from radiative transfer assumptions.

Caveats aside, a number of leaf angle archetypes (simple analytical expression representing particular LADs) have been used to model LAD, covering a wide range of observed canopy types (Wang et al. 2007). These include:

- planophile – favouring horizontal leaves
- erectophile – favouring vertical leaves
- spherical – distributed as if leaves were distributed parallel to the surface of a sphere and so favouring vertical over horizontal, but less than erectophile
- plagiophile – favouring leaves with angles mid-way between erect and flat
- extremophile – favouring leaves with angles at either end of the distribution

An alternative, more general approach has been to use ellipsoidal leaf angle distributions (Campbell 1986; Flerchinger and Yu 2007). These tend to give improved solutions for absorption, but at the cost of more complex models. Hence large-scale remote sensing and Earth system model applications strongly favour the simpler approaches due to the requirements for speed.

A more flexible alternative to specifying archetypes, is to use a parameterisation of $g_l(\theta_l)$ which covers the same variation as these archetypes. Bunnik (1978) proposed a simple four-parameter combination of geometric functions; Goel and Strebel (1984) used a two-parameter Gamma function. The Bunnik (1978) model is shown in Eq. 11.11 (assuming $g_l(\theta_l)$ is independent of azimuth)

$$g(\theta_l) = \frac{2}{\pi}[(a + bcos(2c\theta_l)) + dsin\theta_l] \quad (11.11)$$

Examples of the behaviour of the Bunnik model are shown Fig. 11.3. The fixed archetypes of Ross (1981) agree with these parameterisations very closely across all angles. The uniform distribution (not shown in Fig. 11.3) i.e. randomly-distributed leaf normals, is often assumed for simplicity but is rarely seen in practice.

The turbid medium approximation permits a description of canopy scattering as a function of a small number of structural parameters. Various models have been based on the approach outlined above originating from the work of Monsi and Saeki (1953). The major assumption underpinning Beer's Law is that the number of scattering objects in a volume of canopy (leaves, stems etc.) is proportional to its volume. However, Knyazikhin et al. (1998) show that the canopy structure may in some cases be fractal, resulting in non-linear relationships between canopy volume and the density of scattering elements, violating the assumptions of Beer's Law. However, the basic formulation of Beer's Law can be a useful tool in describing single scattering interactions within the canopy (Monsi and Saeki 1953). This issue of non-random spatial distribution of canopy material (clumping) is discussed further below.

A major drawback of the turbid medium approximation is that the size of the scattering objects within the canopy is not considered. By definition, the canopy is assumed to

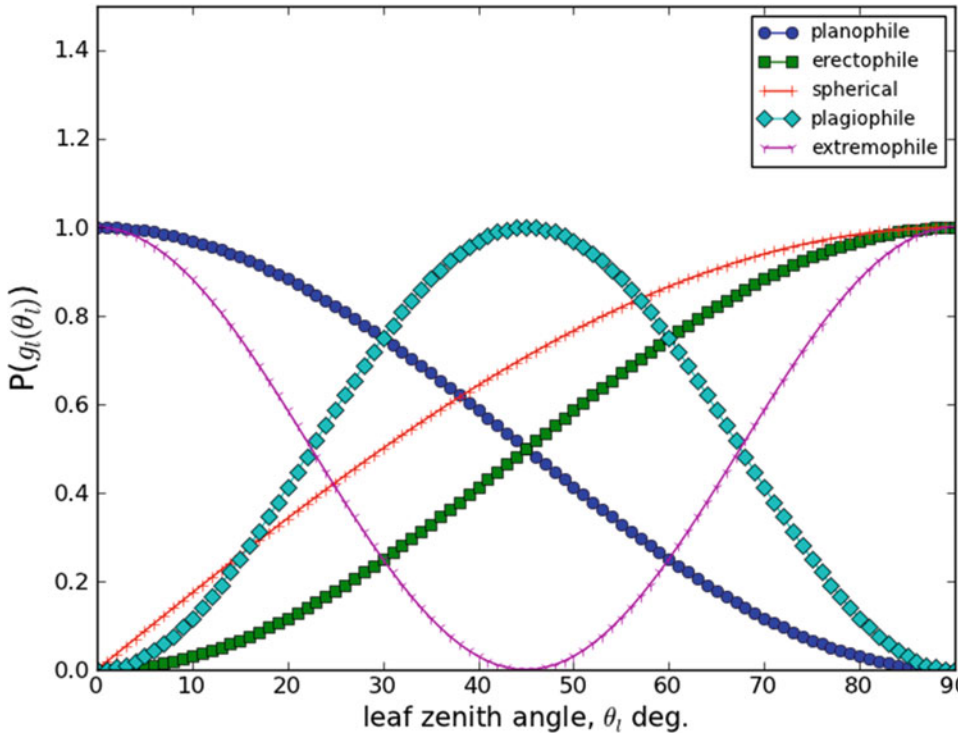


*Fig. 11.3.* Examples of (normalized) leaf angle distribution functions generated using the Bunnik (1978) four parameter model with parameter value sets: (1, 1, 1, 0), (1, −1, 1, 0), (0, 0, 0, 1), (1, −1, 2, 0) and (1, 1, 2, 0) in legend order

be a homogeneous medium of infinitesimal scatterers (to satisfy the far-field approximation) with mutual shading not permitted. Consequently, expressions describing the reflected radiation from such a canopy do not contain information regarding the size of scattering objects. However, certain properties of observed canopy scattering are directly controlled by the size and orientation of scattering objects (e.g. Pinty et al. 1989). A canopy-level example of this impact of finite leaf size is the hotspot effect. At the leaf level, the penumbra effect is of particular importance to photosynthesis, which depends very strongly on the leaf-level irradiance. The penumbra effect describes the fact that irradiance at the leaf is neither wholly direct nor diffuse, but somewhere in between, a consequence of the finite size of both the solar disk (light rays are never perfectly parallel) and the leaf (Cescatti and Niinemets 2004). Turbid medium approximations will not capture such features, and if the size of scattering objects is to be considered a different approach is needed to model the dimensions of scattering elements explicitly (Myneni et al. 1989).

As we can see, solving the radiative transfer equation in a vegetation canopy is a complex problem. Inverting the resulting models must generally be performed numerically, or using look-up-tables. Additionally, the approximations made in order to solve Eq. 11.2 result in the model driving parameters being relatively 'far-removed' from parameters directly representative of physical canopy properties. This issue of so-called 'effective parameters' is critical to applications of remote sensing and is discussed further below. First, I look at how radiative transfer is considered at the leaf level. Following this, a relatively new approach to radiative transfer modelling is outlined,

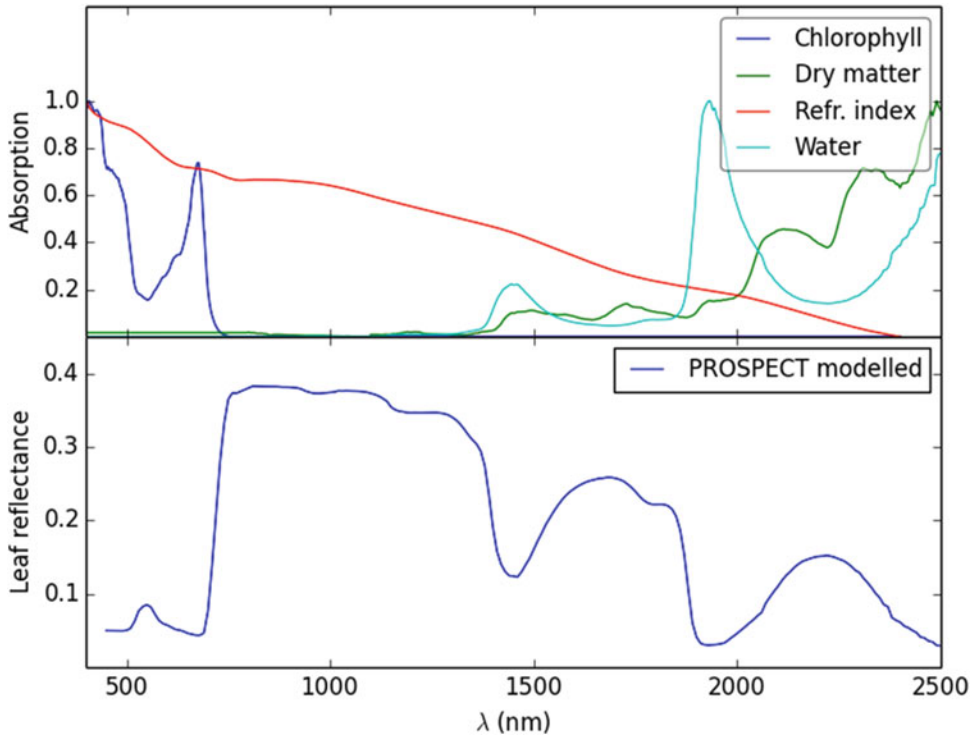


*Fig. 11.4.* Normalized absorption coefficients used within the PROSPECT model (*upper panel*) and leaf spectral reflectance modelled by PROSPECT from these absorbing constituents (*lower panel*)

which scales from leaf to canopy, and has significant consequences for understanding the links between canopy structure and biochemistry.

### *C. Radiation Transfer Within the Leaf*

Now we have a description of radiation transfer in a canopy, the issue arises of radiation interactions at the scale of leaves. This problem is analogous to the canopy case: radiation can penetrate the air/surface interface depending on the surface properties Ross and Marshak (1989) (waxy, smooth etc.) and can either pass through air gaps within the leaf unimpeded or be scattered, across cell walls into and through cells, as well as at the boundaries between cells and cell/air. Scattering within the leaf will depend on the amount of material encountered by a photon (function of leaf thickness, analogous to leaf area density at the canopy level) and the absorption properties of the materials(s), typically the concentrations of absorbing pigments (chlorophyll, carotenoids, flavonoids), water and other absorbents such as lignin and cellulose. It is the pigments, and their relationships to leaf/canopy state and nutrient concentrations (particularly leaf N), that are often of interest via remote sensing (Ollinger 2011).

Various approaches to modelling radiative transfer within the leaf have been proposed and Jacquemoud and Ustin (2008) provide an excellent overview. Leaf models require at the very least some description of the refractive index (essentially a structural effect, modifying behaviour at boundaries of scattering materials within the leaf such as cell walls, air and water etc.), and the specific absorption coefficients of absorbing constituents within the leaf. Examples of these properties taken from the widely-used PROSPECT model of Jacquemoud et al. (1996) are given in Fig. 11.4 along with a modelled leaf spectrum for comparison.

This illustrates the very specific wavelength ranges over which the absorption properties act: chlorophyll pigment dominates the visible; refractive index (leaf structure) dominates beyond this into the NIR; water and to a lesser extent dry matter (such as cellulose and lignin) dominate beyond 1300 nm. In the UV region, proteins, tannins and lignin are important, but these regions are rarely used in large-scale remote sensing due to the absorption of the solar signal by the atmosphere.

Leaf radiative transfer models essentially follow one of four broad schemes. The first and perhaps simplest approach considers a leaf as a semi-transparent plate with plane parallel surface, and some surface roughness (Allen et al. 1969). Scattering from the leaf is calculated as the total sum of successive orders of scattering from reflections and refractions at the plate boundaries with the air. This approach has been generalised to consider multiple plane parallel plates by decomposing the total upward and downward fluxes (a two-stream approach) into the separate fluxes from each plate (Allen et al. 1970). This latter approach is used in PROSPECT, perhaps the most widely-used leaf radiative transfer model for remote sensing applications. The model has developed over a number of iterations through inclusion of more detailed treatment of absorption coefficients in particular (Feret et al. 2008). PROSPECT has been used to explore the impact of biochemistry on leaf reflectance, to infer optical properties from remote sensing measurements, and been coupled to canopy radiative transfer schemes (Jacquemoud et al. 2009).

An alternative approach for modelling radiative transfer properties of leaves that do not conform to the plane parallel approximation, such as needles, has been to consider scattering from discrete particles such as spheres. The LIBERTY model of Dawson et al. (1998) follows this approach, using the formulation of Melamed (1963) for scattering from suspended powders. Particle size is assumed $\gg\lambda$, and scattering is again a function of successive internal reflections and refractions, but from within spheres in this case, rather than plates.

One of the difficulties in developing and testing leaf models has been the concomitant difficulty of measuring leaf optical properties, either in the lab or the field. Measurement equipment has certainly improved in recent years, with the development of portable field spectrometers and integrating spheres. However, leaf measurements are still challenging as they involve handling and mounting leaf material without damaging it, controlling environmental lighting conditions, making reference measurements etc. Thus the number of high quality leaf measurements that can be used for testing models, particularly for needles, or non-flat leaves is rather small (see for example Hosgood et al. 1995).

A range of more general radiative transfer modelling approaches have been proposed for the particular size problem of leaves. One solution of this class is the development of Kubelka-Munk theory to provide a 2- or 4-stream approximation to represent the upward and downward fluxes (separated into diffuse and direct in the 4-stream case) within a single leaf layer, or multiple layers (Vargas and Niklasson 1997). This type of model has the advantage of allowing analytical solutions in certain specific cases. An alternative is to solve the radiative transfer problem numerically, via Monte Carlo methods (described in Sect. E in more detail). Govaerts and Verstraete (1998) demonstrated the use of a Monte Carlo ray tracing (MCRT) model which considered the internal structure of the leaf explicitly in 3D. Baranoski (2006) developed a variant of MCRT for bifacial leaves that calculates Fresnel coefficients for all interfaces in the leaf (air, adaxial and abaxial epidermis, mesophyll cell walls and cytosol), and uses these coefficients to weight Monte Carlo samples of reflectance and transmittance; scattering within a cell is approximated by Beer's Law. The main advantage of these more structurally detailed approaches is

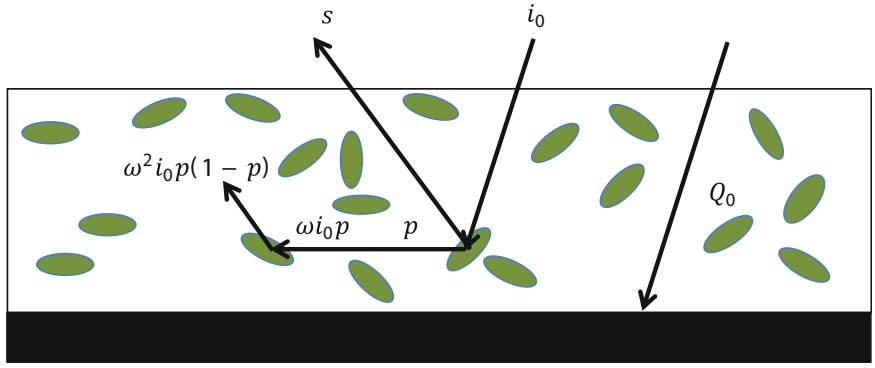


*Fig. 11.5.* Schematic representation of radiation that passes through the canopy uncollided ($\boldsymbol{Q_0}$), or is first intercepted by the canopy ($\boldsymbol{i_0}$) or escapes in the upward direction ($\boldsymbol{s}$) to be measured. $\boldsymbol{p}$ is the probability of a scattered photon being re-intercepted and $\boldsymbol{\omega}$ is the leaf single scattering albedo (After Lewis, P. http://www2.geog.ucl.ac.uk/~plewis/CEGEG065/rtTheoryPt1v1.pdf)

flexibility. The main limitation is the requirement for information to parameterize the model, such as cell dimensions, air volumes etc. Such models can be used to explore the impact of structure at the canopy level on issues such as the relative absorption of diffuse to direct light (Alton et al. 2007; Brodersen et al. 2008), as well as at the leaf level, where surface and internal properties, such as polarization and focusing may be important (Martin et al. 1989; Combes et al. 2007).

The following section describes relatively new developments in solving the canopy radiative transfer problem that have provided new parameterisations of multiple scattering that apply across scales from within-leaf to canopy. These methods have already been applied successfully to the problem of modelling leaf reflectance (Lewis and Disney 2007) and are providing new insight into the nature of radiative transfer in vegetation more generally.

### *D. Recollision Probability and Spectral Invariance*

As seen above, the key to providing an accurate description of canopy radiative transfer is the multiple scattering component, particularly at NIR wavelengths. Development of the concept of the so-called 'recollision probability' $p$ has seen significant advancement in this area. The approach is summarised in Huang et al. (2007), but is based on the observation that the decrease in scattered energy with increasing scattering interactions is well-behaved and close to linear in log space, at least in canopies with low to moderate LAI (Lewis and Disney 1998). Scattered energy typically decreases dramatically after 1 or 2 interactions, and then proceeds to decrease more slowly with increasing scattering order. This implies that, once the scattering reaches the linearly decreasing portion, the scattering at interaction order $i+1$ is simply $p$ times the scattering at interaction order $i$. Figure 11.5 illustrates this situation schematically.

From Fig. 11.5 we can see that some proportion of the incoming radiation $Q_0$ may pass through uncollided to the lower boundary layer. If this layer is assumed completely absorbing (black soil, a reasonable approximation for dense understory and/or dark soil), then multiple scattered radiation can only originate from vegetation. The first interaction with leaves is then $i_0 = 1 - Q_0$. A fraction $s$ of this scattered radiation exits the canopy in the upward direction, and the remaining proportion $p$ interacts further with leaves in the canopy. Therefore the first order scattered radiation is $s_1 = i_0\omega(1\text{-}p)$ where $\omega$ is the leaf single scattering albedo. Rearranging, we obtain $s_1/i_0 = \omega(1\text{-}p)$. The probability of being further intercepted is also $p$, so the second order scattering

$s_2 = \omega p s_1 = i_0 \omega^2 p(1\text{-}p)$. Following the same logic for higher orders we see that

$$\frac{s}{i_0} = \omega(1-p) + \omega^2(1-p)p + \omega^3(1-p)p^2 + \cdots = \omega(1-p)[1 + \omega p + \omega^2 p^2 + \cdots] \tag{11.12}$$

The series in $p$ and $\omega$ can be summed as

$$\frac{s}{i_0} = \frac{\omega(1-p)}{1-p\omega} \tag{11.13}$$

This provides for a very compact description of multiple scattering, albeit under the assumptions of total scattering and black soil. Crucially, the resulting scattering is *independent of wavelength* i.e. is spectrally invariant, and is a function of $p$ only, where $p$ is a purely structural term, encapsulating the size and arrangement of scattering elements within the canopy. Recollision theory has been developed over the last decade (Knyazikhin et al. 1998, 2011; Disney et al. 2005; Huang et al. 2007). It has been shown to work well for higher values of LAI when the understory becomes less important (Huang et al. 2007). This is also where optical EO tends to be less sensitive to variations in LAI. The recollision probability approach has now been used for a range of remote sensing applications including in a parameterised canopy model (Rautiainen and Stenberg 2005), to classify forest structural types (Schull et al. 2011), and for providing a structural framework for merging data from various sensors with different spatial and spectral resolutions (Ganguly et al. 2008, 2012). Further, the same behaviour has been observed in atmospheric radiative transfer (Marshak et al. 2011).

Specific insights provided from the spectral invariant approach include that of Smolander and Stenberg (2005) who showed that if the fundamental scattering element within a canopy is considered to be a shoot (a good approximations in conifers for example), then a shoot-level recollision probability $p_{shoot}$, can be defined. In this case total scattering can be expressed as a nested combination of the within-shoot needle-level recollision probability, $p_{needle}$ and $p_{shoot}$. This is a key insight into how different scales of clumping interact. Following this, Lewis and Disney (2007) used recollision probability to parameterise the PROSPECT leaf-level radiative transfer model. Their rephrasing in terms of $p_{leaf}$ was able to reproduce the behaviour of PROSPECT with very high accuracy (root mean square error $<$0.4 % across all tested conditions). Lewis and Disney (2007) also showed that the same form of scattering will be nested across multiple scales from within-leaf to shoot to canopy. A key implication of this work was the observation that the structural and radiometric components of the canopy (represented by $p$ and the leaf absorbing constituents such as pigments, cellulose, lignin, and water) are fundamentally coupled. As a result Lewis and Disney (2007) conclude "...it is simply not possible to derive robust estimates of both leaf biochemical concentration and structural parameters such as LAI from (hyperspectral) data ... no matter how narrow the wavebands or how many wavebands there are". Increasing LAI by some factor $k$ and simultaneously decreasing the biochemical concentration per unit leaf area by the same factor (i.e. keeping the total canopy concentration the same) can result in the same total scattering, but for very different values of $p$, corresponding to very different canopy structures. This implies that without knowledge of either $p$ or the leaf biochemical constituents, independent retrieval of either from total scattering measurements is not possible. An additional implication is that attempts to estimate 'total' canopy biochemical concentration as a coupled measure may contain large errors.

The various developments of recollision probability have important implications for the use of Earth observation data to infer canopy biochemical properties, particularly pigment concentrations. Many studies have observed empirical correlations between canopy biochemical concentrations and observed spectral properties (reviewed by

Ollinger 2011), including observed positive correlations between leaf nitrogen content per area (canopy N) and albedo. Such work suggests a potentially important route for monitoring canopy biochemistry (and hence state) from EO. However, recent work by Knyazikhin et al. (2013) building on recollision probability theory and the observation that $p$ encapsulates scattering across scales, shows quite clearly that some of these correlations e.g. between canopy N and albedo, are in fact entirely explained by canopy structure. As an example, Knyazikhin et al. (2013) show that observed correlations between canopy N and reflectance (e.g. Ollinger et al. 2008) can be almost completely explained by canopy structure. Knyazikhin et al. (2013) also suggest that canopy scattering can be reformulated using recollision probability, as a combination of separate structural and spectral terms as follows:

$$BRF_\lambda(\mathbf{\Omega}) = DASF \cdot W_\lambda \tag{11.14}$$

where $DASF$ is the (structural) Directional Area Scattering Factor and $W_\lambda$ is the (spectral) canopy scattering coefficient. DASF is defined as:

$$DASF = \rho(\mathbf{\Omega})\frac{i_0}{1-p} \tag{11.15}$$

where $\rho(\mathbf{\Omega})$ is the directional gap density of the canopy, along a given viewing direction $\mathbf{\Omega}$; $i_0$ is the first interception by the canopy from Eq. 11.14. $W_\lambda$ is defined as:

$$W_\lambda = \hat{\omega}_\lambda \frac{1-pi_\mathrm{L}}{1-\hat{\omega}_\lambda pi_\mathrm{L}} \tag{11.16}$$

where $i_\mathrm{L}$ is the leaf interceptance defined as the fraction of radiation incident on the leaf that enters the leaf interior; and $\hat{\omega}_\lambda = \omega_\lambda / i_\mathrm{L}$. The quantity $\rho(\mathbf{\Omega})LAI$ is the fraction of leaf area inside the canopy visible from outside the canopy along $\mathbf{\Omega}$. For dense canopies in the NIR, $DASF \sim \rho(\mathbf{\Omega})LAI$ and is an estimate of the ratio between the leaf area that forms the canopy boundary as seen along $\mathbf{\Omega}$ and the total (one-sided) leaf area, effectively the 'texture' of the canopy upper boundary. Importantly, calculating $DASF$ allows the impact of structure to be removed from observed hyperspectral reflectance, providing a potential route for re-analysis of empirical relationships between biochemistry and reflectance.

The recollision probability theory has provided new ways to express scattering across scales, and has found a range of potential applications in accounting for structural effects in EO measurements. Ustin (2013) highlights the importance of using a first principles radiative transfer approach to accounting for the impact of structure on EO estimates of biochemistry.

### *E. 3D Monte Carlo Approaches*

The methods outlined above to solve the radiative transfer problem in vegetation involve a range of approximations regarding structural and radiometric properties in order to make the problem tractable. A sub-class of methods exist which solve the radiative transfer problem based on 'brute force' Monte Carlo sampling of the radiation field in a 3D canopy. These methods derive from developments in computer graphics, where they form the basis of modern movie animation and special effects. The aim in these applications is to simulate 'realistic' light environments i.e. scenes that are either convincing and/or aesthetically pleasing to the human eye. For EO applications, the requirement is somewhat different i.e. physical accuracy (including constraints such as energy conservation for example). Monte Carlo methods are computationally intensive, which has tended to limit their application. However, computing power has reached a level where such limitations are no longer so relevant, and these methods have some key advantages for quantitative applications. Niinemets and Anten (2009) discuss the issues of the trade-off between accuracy

and efficiency in radiative transfer modelling approaches.

Monte Carlo methods in remote sensing are reviewed in detail by Disney et al. (2000) and Liang (2004). These methods fall into two broad classes: radiosity (originating from thermal engineering), which requires calculating the viewed areas of each object in a scene in relation to the other objects in the scene (so-called 'view factors'); and ray tracing (MCRT). I will briefly discuss the latter method here, as it is more practical for EO applications where view and illumination configurations change arbitrarily (making radiosity less feasible). MCRT essentially involves calculating the intersections of photons (rays) projected into a 3D scene with the objects in the scene, and determining the behaviour of these photons at each intersection. The subsequent direction and energy of a scattered photon following an intersection is governed by the radiometric properties of absorption, transmission and reflection of the surface at the point of intersection, in addition to the geometric scattering properties (phase function) of the object. Objects are not limited to representation by simple polygons (facets). Volumetric objects can be used, in conjunction with a description of the (volumetric) scattering properties of the materials contained within (North 1996). Diffuse sampling can be used to simulate diffuse light sources (Govaerts 1996; Lewis 1999). The bidirectional reflectance of a given scene (represented as a collection of 3D objects) is simulated by simply repeating the sampling process for every sample (pixel) in the viewing plane (Disney et al. 2000), possibly multiple times.

A key advantage of MCRT models is that they can operate on structurally explicit 3D scenes, often of arbitrary complexity, allowing them to simulate EO signals with the least possible number of assumptions about structure. Some models represent 3D detail in a given scene down to the level of individual needles and leaves (España et al. 1999; Lewis 1999; Govaerts and Verstraete 1998; Widlowski et al. 2006). Other approaches represent larger structural units explicitly such as tree crowns, but then make assumptions regarding the scattering and extinction properties within individual crowns (North 1996). The issue with this latter approach is determining what these within-crown bulk scattering properties ought to be. Other models divide 3D space into voxels, and assign voxel-average scattering properties, such as the Discrete Anisotropic radiative transfer (DART) model of Gastellu-Etchegorry et al. (2004). This has benefits in terms of speed and simplicity, but again at the expense of requiring definitions of bulk (volume) scattering properties. Fully explicit 3D MCRT models avoid these volume scattering approximations, but at the expense of requiring 3D input on all canopy elements, as well as potentially much greater computational demands (Disney et al. 2006; Widlowski et al. 2013).

The ability to deal with 3D canopy structure explicitly means MCRT models are ideally-suited to applications where we wish to know, and have control over, 3D scene properties in order to generate a modelled EO signal e.g. for generating synthetic data sets to test retrieval algorithms based on simpler model approximations or when EO data are not readily available. Disney et al. (2011) show how 3D MCRT model simulations can be used as a surrogate for observations of fire impact. Other applications include simulating the properties of new sensor characteristics (Disney et al. 2009); understanding the impact of structure on observations (España et al. 1999); providing a common structural framework for combining optical and microwave scattering models (Disney et al. 2006); and providing benchmark information for testing simpler radiative transfer models (Widlowski et al. 2007). This latter example is an important one; a question that arises for anyone using any radiative transfer approach to an EO application is: which model is best for my application, and why? The Radiation Transfer Model Intercomparison exercise (RAMI, http://rami-benchmark.jrc.ec.europa.eu/HTML/) has sought to answer this question via intercomparison of radiative transfer models. Over various phases RAMI has shown that detailed 3D MCRT models can

provide the most credible solution to the radiative transfer problem in well-defined, simplified cases (Widlowski et al. 2007). Scenes can be defined for which MCRT models provide exact solutions (within limitations of numerical sampling), and this allows for testing of more approximate radiative transfer models, in particular quantifying the impact of model assumptions on resulting model accuracy. The RAMI work has led to an online benchmarking tool, allowing radiative transfer model developers to test and benchmark their models (Widlowski et al. 2008). The most recent RAMI exercise has shown how detailed 3D MCRT models can represent the effects of structure on the EO signal for very complex (realistic) 3D scenes in ways that simpler models cannot (Widlowski et al. 2013).

There are three main limitations of the MCRT approach. First, they are very slow compared to the more approximate models. This is certainly a problem if speed is absolutely essential, e.g. for large-scale or near real-time applications. MCRT models can of course still be used to quantify the impact of assumptions made in simpler models. Secondly, they cannot be inverted either directly or using standard optimisation routines, given their requirement for explicit location and properties of a (potentially) very large number of 3D objects. However, computation speeds have increased to an extent where it is now feasible to consider using a MCRT model for look-up table-based model inversion. It may take thousands of hours of CPU time to run forward MCRT model simulations over a large range of canopy, view and illumination configurations to populate the pertinent look-up tables, but these need only be run once. The third and perhaps most serious limitation of 3D MCRT models is that they are only as good as the underlying 3D scene descriptions on which they are based; the models require highly-detailed, accurate 3D structural information to generate 3D model scenes. This 3D information can come from various sources, including empirical growth models (e.g. España et al. 1999; Disney et al. 2006), purely parametric models (Widlowski et al. 2006; Disney et al. 2009), and parametric models modified using field measurements (Disney et al. 2011).

A range of models can provide 3D scene information. Growth models provide an accurate description of a 'domain-average' tree structure, but not a specific tree at a particular time (Leersnijder 1992; Perttunen et al. 1998). Parametric models allow a great degree of flexibility over manipulation of tree structure. Various models of this sort exist, e.g. xfrog (Xfrog Inc. xfrog.com) and OnyxTREE (Onyx Computing, onyxtree.com) and they have been used in EO applications (Disney et al. 2010, 2011). However, it can be both time-consuming and difficult to parameterise a model that is designed to 'look right' for computer graphic visualisation (Mêch and Prusinkiewicz 1996), in such a way that it is a structurally accurate representation of a tree for radiative transfer applications (leaf and branch shape and size distributions, leaf angular distributions etc). An alternative approach is the use of growth grammars based on L-systems (Prusinkiewicz and Lindenmayer 1990). These use simple growth rules to produce 'realistic' canopy structure and have been used to drive 3D simulations, particularly of relatively simple crop canopies (Lewis 1999), but may bear little resemblance to real canopies of greater complexity. Functional structural plant modelling (FSPM) overcomes this limitation to a certain extent by considering fundamental rules of plant function due to the genetic and organ level constraints to drive structural development (Godin and Sinoquet 2005). The resulting 3D structure can in turn be expressed via L-systems. FSPM and L-systems approaches suffer from the same problem that the resulting models are accurate instances of a particular species or plant type, rather than specific (observed) plants. Furthermore, additional rules are needed to create a general, 3D scene.

These limitations on 3D structure have led to searches for new ways to derive detailed,

accurate 3D information that can be used to drive 3D simulation models. Some of these methods are outlined below in Sect. IV.

## III. Effective Parameters

### *A. Basics: Definition of Effective Characteristics*

Having discussed the various approximations that can be employed to help solve radiative transfer equations in leaves and canopies, a note of caution is required in regard to any biophysical parameters we derive from EO data via such methods.

For real canopies the exponent in Eq. 11.6 implicitly includes a structural term $\zeta(\mu')$ encapsulating the fact that real canopies are not turbid media but are clumped at multiple scales from cm to tens of m. Leaves or needles are arranged around twigs, along branches, within crowns and within stands. Pinty et al. (2004, 2006) suggest adopting an effective LAI value $\widetilde{LAI}\,(\mu')$ i.e.

$$\widetilde{LAI}\,(\mu') = LAI\zeta(\mu') \tag{11.17}$$

This permits a solution to the 1D limiting case of radiative transfer in a 3D canopy that is consistent with the assumptions made in Eq. 11.2. Crucially however, the values of $\tilde{LAI}\,(\mu')$ are not the same as $LAI$ which are in turn, not the same as the actual LAI that would be measured on the ground (unless measured over some large, discrete canopy volume). That is, the resulting radiative transfer model parameters will be 'effective' parameters and will not have a direct physically measurable meaning. These effective parameters allow solution of the 1D radiative transfer problem by representing domain-averaged quantities that are forced to satisfy the constraints associated with a 1D representation of what is an inherently 3D system (Pinty et al. 2006).

The issue of effective parameters is important because it encapsulates the problem of interpreting EO measurements more generally. As an example, a typical use of a 1D radiative transfer scheme is to describe the surface radiation budget in a large-scale Earth System Model (ESM) (Sitch et al. 2003; Best et al. 2011). Developing such a model is inevitably a trade-off between multiple and often competing constraints including computational speed and model robustness vs. providing 'sufficiently accurate' radiant flux values (Pinty et al. 2004). Moreover, introducing a physically-realistic estimate of LAI (for example) may only make things worse, as it will not be consistent with the simplified radiative transfer schemes and will thus introduce errors. If radiative consistency is the key requirement (getting the fluxes right) rather than interpreting the LAI values, then the effective parameters should be used (Pinty et al. 2006, 2011a, b). What is true of LAI is potentially true of other structural and biochemical parameters in radiative transfer schemes.

The issue of consistency between EO-derived biophysical parameters, and their representation in models of vegetation function, biogeochemical cycling and climate is key to making best use of both observations and models. The fusion of EO data with models, particularly via data assimilation (DA), is a rapidly-growing field because EO data can potentially provide information on land cover, plant functional types (PFTs), vegetation state and dynamics, land surface temperature (LST), soil moisture etc. at the scales and frequencies required by the large-scale models (Pfeifer et al. 2012). However, the further an EO-derived parameter is away from a fundamental EO measurement, the more likely it is to be 'effective' rather than directly measurable. This in turn increases the likelihood of inconsistency between EO data and large-scale models that use these parameters (Carrer et al. 2012a; Pfeifer et al. 2012).

### *B. Data Assimilation*

As the spatial detail of the land surface representation within ESMs increases (from ~$10^3$ to ~$10^1$ km and finer), the assumption

of canopy homogeneity typically assumed in a simplified radiative transfer approach is violated and potentially becomes an increasing source of error (Knorr and Heimann 2001; Pinty et al. 2006; Brut et al. 2009; Widlowski et al. 2011). Various solutions have been proposed, essentially approaching the problem from opposite directions. From the EO perspective, one approach is to ensure consistency between EO parameters and ESMs as far as possible by coupling a physically-realistic radiative transfer scheme directly to the ESM that will use it. The ESM can then actually predict an EO measurement, which in turn allows direct comparison with EO data. Perhaps more importantly, the model can also be used to assimilate EO data to estimate ESM model state properties (in an inverse scheme). This approach lies at the heart of data assimilation schemes with land surface models (Quaife et al. 2008; Lewis et al. 2012). For a DA scheme, the RT models are referred to as 'observation operators' (denoted $H(\boldsymbol{x})$) which map the model state variable vector $\boldsymbol{x}$ to the EO signal (as a vector) $\boldsymbol{R}$ for a given set of control variables i.e. $\boldsymbol{R} = H(\boldsymbol{x})$. The inverse problem is then to obtain an estimate of some function of $\boldsymbol{x}$, $F(\boldsymbol{x})$ from measurements $\boldsymbol{R}$ (Lewis et al. 2012). An advantage of this approach is that it can utilise much more direct EO measurements (reflectance or even radiance) where the uncertainties in the measurements can be better-characterised. This characterisation of uncertainty (in observation *and* radiative transfer model schemes) is critical for data assimilation. A drawback is that more complex radiative transfer schemes tend to slow the assimilation process, potentially limiting them for large-scale inverse problems (at least currently). However, data assimilation approaches of this sort are being used to assimilate EO data from a range of sources, and have shown great promise in improving and constraining model estimates of C fluxes and photosynthesis (Quaife et al. 2008; Knorr et al. 2010), evapotranspiration (Olioso et al. 2005), surface energy balance (Qin et al. 2007; Pinty et al. 2011a, b) and hydrology (Rodell et al. 2004; Houser et al. 2012).

### *C. Scale Differences and Model Intercomparisons*

From the other direction, we can modify the ESM internal radiative transfer scheme to account for inconsistency with EO measurements and ensure the resulting ESM outputs are consistent at some broader, integrated level e.g. such as total productivity (Brut et al. 2009; Carrer et al. 2012). An example of this is improved representation of canopy diffuse fluxes, which tend to increase C uptake (via increased photosynthesis) with increasing diffuse radiation fraction (Mercado et al. 2009). Carrer et al. (2012) show that introducing clumping to an ESM representation of vegetation (resulting in an effective LAI), even at coarse scale, can improve modelled annual GPP fluxes of various deciduous and conifer forests by up to 15 %. This approach accepts that the resulting internal model parameters are effective and not measurable in practice. Lafont et al. (2012) show that this modification of LAI can have a significant impact on the way fluxes are apportioned within different ESMs.

An additional complication can arise that different internal LAI representations can cause processes such as photosynthesis and transpiration to reach different equilibria (different spatial and temporal distribution of fluxes) in different ESMs while still producing similar net C fluxes i.e. the models can arrive at the same answers for different reasons. This in turn can result in differences in seasonal variations (e.g. timing of peak fluxes) and/or longer-term model divergence that may be hard to identify (Richardson et al. 2012). The effective nature of the model parameters also makes model intercomparison difficult. Clearly, the consideration of scale is not consistent between models.

Recent work by Widlowski et al. (2011) has attempted to address the issue of consistency of radiative transfer schemes in ESMs systematically, by instigating a

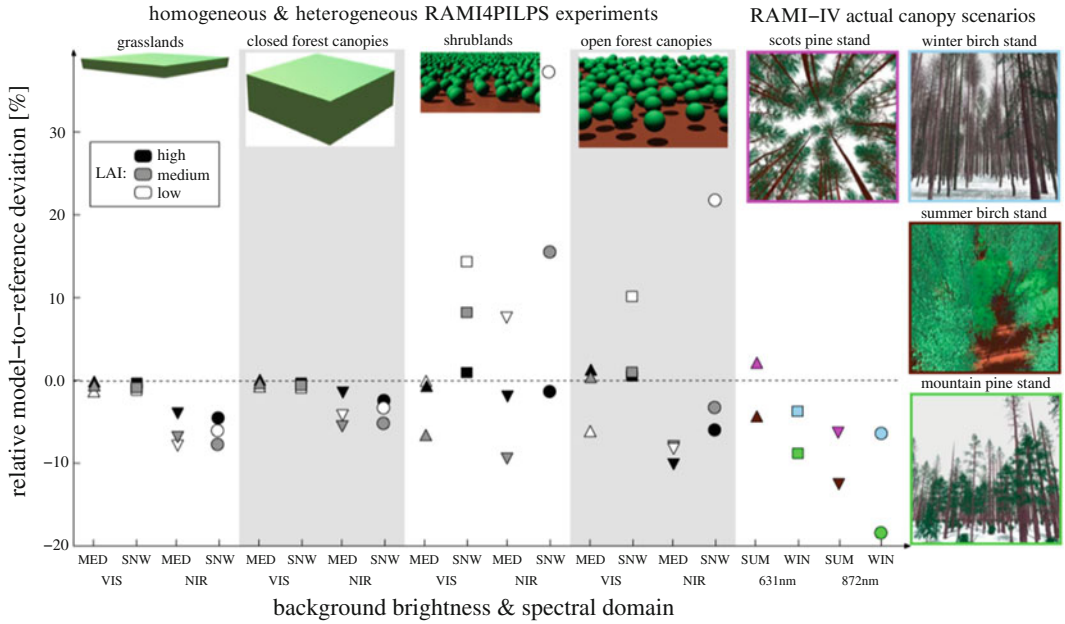


*Fig. 11.6.* An illustration of differences in canopy absorption as a function of increasing structural complexity (from left to right) for visible and NIR spectral domains. Different grey levels show varying LAI (low = 0.5, medium = 1.5, high = 2.5), over snow-covered (SNW) and medium-bright (MED) backgrounds, with $\theta_i = 60°$ or 27° respectively. The first two panels represent simple 1D radiative transfer models; the second two panels represent the most basic level of 3D heterogeneity; the right-most column includes four reference cases derived via a full 3D Monte Carlo Ray Tracing (MCRT) model description (Modified from Widlowski et al. 2011 © Wiley)

radiative transfer model intercomparison exercise, RAMI4PILPS (http://rami-benchmark.jrc.ec.europa.eu/HTML/RAMI4PILPS/RAMI4PILPS.php). RAMI4PILPS builds on both the RAMI exercise and the Project for Intercomparison of Land Surface Parameterization Schemes (PILPS). PILPS was set up to improve understanding of model processes in coupled climate, atmospheric and ESMs mainly through intercomparison of the various model parameterisation schemes (http://www.pilps.mq.edu.au/). PILPS recognises that for large, complex models, the wide range of approximations and possible parameterisations required makes direct model-to-model comparisons very difficult and instead compares the abilities of the models to reproduce various observed climate and land-surface trends (Henderson-Sellers et al. 2003). RAMI4PILPS is perhaps much closer to RAMI than PILPS in terms of the intercomparison approach. It attempts to isolate the radiative transfer schemes in participating models in such a way as to examine only that part, making like-for-like comparisons much more feasible over specific scenarios. In this case the RAMI results are used to provide a 'known' reference solution. RAMI4PILPS covers quite a large range of model types, from simple land surface model schemes, to very complex models that describe the full range of surface energy, water and C fluxes between the surface and atmosphere. Figure 11.6 shows a comparison of the RAMI4PILPS models against the reference solution for a range of canopy complexities. This comparison demonstrates that the relatively simplistic concept of canopy 'structure' (from varying 1D homogeneous, to a simplified consideration of clumping) can still introduce a large degree of scatter between the models, as well as between the models and the reference solution under different environmental conditions and for different spectral regions.

## IV. New Observations of Structure and Function

Lastly, I discuss newer Earth observation techniques that provide rapid and detailed information on canopy structure and function. These new technologies based on lidar (light detection and ranging) and microwave RADAR (radio detection and ranging) are becoming increasingly widely available. I show that lidar is a near-direct remote sensing measurement of canopy height and structure. There is significant promise in merging airborne lidar scanning (ALS) instruments, and terrestrial laser scanning (TLS) instruments, as well as optical and RADAR data in order to maximise structural information. The 3D nature of the lidar signal also raises the possibility of using these data to further extend and exploit the recollision probability approach to the canopy radiative transfer problem.

I also briefly consider the prospects for EO data of this sort over the next decade, and how such observations might be used. Having discussed new structural measurements, I turn lastly to a new measurement related to canopy function based on chlorophyll fluorescence.

### *A. Structural Information from Lidar and RADAR*

Lidar systems have become increasingly common over the last decade. Figure 11.7 illustrates this by highlighting the increase in published papers with the words "lidar" and "vegetation" in the title or abstract, from 1990–2012. The advent of airborne lidar scanning (ALS) instruments, terrestrial laser scanning (TLS) instruments, and the lifespan of the only spaceborne lidar mission to date used for terrestrial applications (NASA ICESAT/Glas) are marked on the figure (Fig. 11.7).

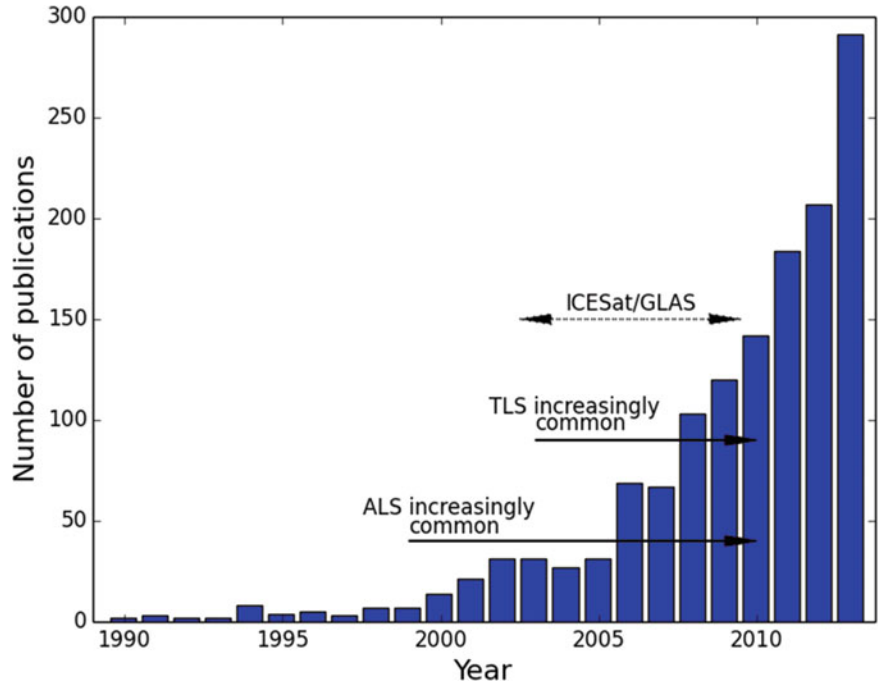


*Fig. 11.7.* Number of publications containing the words 'lidar' and 'vegetation' in the title or abstract from 1990 to 2013 (Citation information from Thomson Reuters Web of Knowledge ©). ALS and TLS are airborne and terrestrial lidar scanning respectively

Lidar is an active remote sensing method, recording return time-of-flight of a laser pulse between instrument and target. Lidar provides a (near) direct estimate of surface (canopy) height and is in this sense a much more direct measurement than those relying on passive reflected or emitted radiation. Lidar instruments also record returned signal intensity and, in combination with height, this signal can provide unique information on the vertical distribution of canopy structure when operated from above the canopy (e.g. Dubayah and Drake 2000). As discussed above, structure plays a critical role in radiative transfer in vegetation. Thus, structure must be accounted for to allow retrieval of canopy state and function from remote sensing. Lidar has proven extremely useful in addressing this issue (Lefsky et al. 2002; Armston et al. 2013a).

#### 1. Discrete-Return Lidar Systems

Lidar systems broadly fall into one of two categories – discrete-return, or full-waveform (the less widely-used phase-based systems are not discussed here). Discrete return lidar essentially records the distance to the first object from which a return is recorded at the sensor, over some signal threshold, or multiple thresholds. Assuming that emitter and detector are co-located, the time-of-flight to the target is $t = 2d/c$ where d is the distance to the target, and c is the speed of light (and assuming that emitter and detector are co-located). For a sensor above a vegetation canopy returns may come from both the canopy and the ground, depending on canopy cover. It is then possible to determine the height of the vegetation canopy, $h$, through the difference in travel time between the two returns i.e. $h = (t_1\text{-}t_2)c/2$. Discrete return lidar datasets therefore comprise 'point clouds', each of which has a 3D co-ordinate relating its location to the sensor. Lidar has been widely used in this way to estimate biomass via allometric relationships with canopy height (e.g. Asner et al. 2010; Asner and Mascaro 2014). Lidar measurements can be used to estimate biomass over dense, high biomass (high LAI) tropical forests where passive optical measurements saturate and are thus insensitive to change and/or variation (Saatchi et al. 2011). Canopy height estimation from lidar is now included in routine commercial and forestry measurements (Næsset et al. 2004; Hyyppä et al. 2008).

#### 2. Full-Waveform Lidar Systems

Waveform (often referred to as 'full-waveform') lidar systems record a 'binned' and digitised version of the real intensity return detected by the sensor, resulting from an outgoing pulse of known form (Mallet and Bretar 2009). Waveform instruments record the intensity of the response at a certain sampling rate (this sampling and detector non-linearity mean that the measurement never are true *full*-waveform), while performing minimal pulse-detection methods. Waveform lidar is becoming prevalent in airborne systems, even if they are in practice often used as discrete return systems with much of the intermediate waveform information being ignored. However, the power of waveform lidar is that it has the capability to record detailed information on the vertical distribution of canopy structure, and hence has a range of applications in remote sensing of vegetation including height and biomass (Dubayah et al. 2010), LAI (Tang et al. 2012) and canopy gap fraction (Armston et al. 2013a). The waveform signal can not only identify where there is a surface, but also what the properties of that surface are. This is particularly relevant for example in distinguishing woody from leaf material. Figure 11.8 shows an example of a modelled full-waveform lidar return over a conifer canopy, and highlights the potential information content of the signal.

#### 3. Limitations and Future Developments of Lidar Systems

A current limitation of lidar is the lack of wide area coverage due to reliance on airborne platforms. However, ALS survey costs

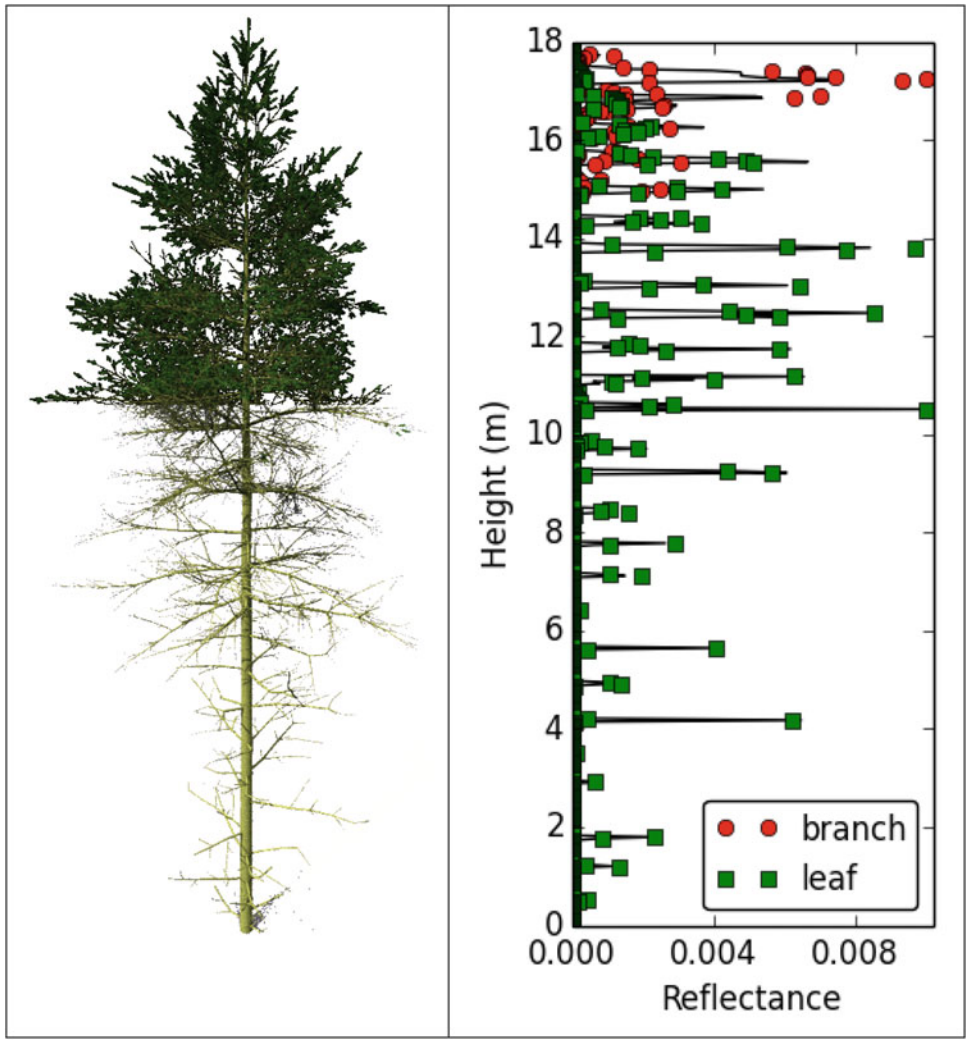


*Fig. 11.8.* Example of full-waveform lidar signal simulated from a 3D model of a Scots pine (*Pinus sylvestris*) tree (visualised in the *left panel*). The signal shows height-resolved return intensity (*black* impulses), as well as the normalized proportion of the signal in each height bin coming from the leaf and branch objects in the 3D model. Leaf and branch returns can be separated explicitly in the 3D model returns

are coming down (Wulder et al. 2012), and so larger and larger areas are being covered, with a number of countries now aiming to obtain total coverage (e.g. see http://www.gim-international.com/issues/articles/id1664-Swedish_Lidar_Project.html).

Obtaining this coverage is time-consuming (typically months to years) and hence can only provide a temporally fragmented 'snapshot' (note that this is only a limitation for very large areas; smaller regions, even 1000s of ha, where forest height and density will not vary in a few weeks or even months, can be covered rapidly and even revisited). In addition, these relatively large surveys are generally designed for deriving digital elevation models (DEMs) rather than for vegetation applications. As a result the sampling is often at or below 1 pt $m^{-2}$ in order to reduce the survey time, meaning limited sampling of the canopy properties. A further difficulty is differentiating between leaf and woody material, particularly in larger footprint instruments. It has been proposed that this

limitation could be overcome by dual wavelength systems using spectral contrast to distinguish canopy components (Morsdorf et al. 2009). No system of this sort has been flown as yet, although work on laboratory prototypes show great promise (Woodhouse et al. 2011). An ongoing issue in dealing with lidar systems of all types is the often proprietary (and hence generally hidden) nature of the instrument characteristics (Disney et al. 2010). This makes it hard to obtain information on key technical specifications such as the thresholds used to trigger a recorded pulse (Armston et al. 2013a), or the stability of the instrument absolute response (and gain). Lidar instruments are rarely if ever calibrated to provide absolute reflectance, making it hard to make quantitative comparisons of signal returns from different backgrounds and canopy types.

In terms of spaceborne lidar for vegetation applications, unfortunately none currently exist due to perceived cost and technical limitations. This is despite the success of NASA's ICESAT/GLAS mission, which is remarkable given that it was not designed for vegetation applications and had some severe limitations including a large footprint (70 m), limited vertical resolution and relatively poor spatial sampling (hundreds of meters along tracks between footprints and kilometres between tracks horizontally). Despite this, GLAS data have been widely used to derive estimates of canopy height and structure over large areas, particularly for tall boreal and tropical forests (Harding and Carabajal 2005; Lefsky et al. 2005; Rosette et al. 2005) as well as forming the basis of the current best estimates of pan-tropical forest biomass (Saatchi et al. 2011; Baccini et al. 2012). A second ICESAT mission is due to launch in 2017 (http://icesat.gsfc.nasa.gov/icesat2/) but will have a different lidar system to that on ICESAT, and the possibilities for vegetation applications are as yet uncertain. Future prospects for space-based canopy lidar improved in July 2014, when NASA announced plans to launch the Global Ecosystem Dynamics Investigation (GEDI) lidar system on board the International Space Station (ISS) in 2019.

#### *4. Terrestrial Laser Scanning (TLS)*

Another development over the last decade has been the rise of terrestrial laser scanning (TLS) instruments. Typically developed for commercial surveying applications, TLS data have proved an interesting source of 3D canopy structure information (Maas et al. 2008). Given the importance of 3D structure for radiative transfer modelling, biomass, canopy state etc., ways to rapidly and accurately characterise structure are obviously attractive. This is particularly true as traditional field-based measurement of structure are hard to make, particularly in remote and tall forests where access may be limited. Under these conditions, even measuring tree height can be problematic. As a result, structural measurements are often limited to diameter-at-breast height, stem number density, with perhaps some estimates of overall height, height-to-crown ratio, and crown extent. Tree height can be estimated using hypsometers or clinometers and even cheap laser ranging devices. However, for these height measurements, the top of a tree has to be visible from the ground. In dense canopies, with tall trees or in steep terrain, this can be problematic. Additional structural measurements are often inferred from indirect techniques, such as gap fraction and cover (and hence LAI) from upward-looking hemispheric photographs. TLS can potentially overcome many of these limitations, allowing rapid estimation of dbh, height and vertical structure and potentially providing information that can be used to develop 3D canopy structural models quickly and accurately (Raumonen et al. 2013).

The value of TLS measurements has seen development of new instruments specifically designed for vegetation applications, including: the use of wavelengths that are eye-safe, but also reflected strongly by vegetation (e.g. 1064 nm); a move from discrete-return to

waveform instruments; full hemisphere scanning; multiple wavelengths. Most of these innovations have been developed in the research community, but commercial manufacturers are now recognising there may be a larger market for robust field-portable vegetation TLS instruments. Perhaps the most exciting of these developments is that of full-waveform, hemispherical scanners, with dual wavelengths. The only currently operational instrument is the Salford Advanced Laser Canopy Analyser (SALCA), which operates at 1040 and 1550 nm (Danson et al. 2014). As for ALS, dual wavelengths have the potential to allow leaf and woody material to be separated in the lidar scans (Woodhouse et al. 2011). Another new instrument is the dual-wavelength Echidna laser scanner (DWEL, Douglas et al. 2012), a development of the Echidna single wavelength instrument that has been deployed successfully for a number of canopy applications (Yao et al. 2011). Both SALCA and DWEL are prototypes and require significant time to set up and carry out full hemisphere scans. A more robust, commercial alternative is the Riegl VZ-400 scanner (http://www.riegl.com/uploads/tx_pxpriegldownloads/DataSheet_VZ-400_18-09-2013.pdf). This is a full waveform hemispherical TLS instrument, albeit with a single wavelength at 1550 nm. It is a robust, field-ready instrument that can carry out high angular resolution hemispherical scans in 1–2 min. It can be used in conjunction with a digital camera to provide image data aligned to the scan data to aid target identification (and even separation of canopy elements). The instrument was not designed for vegetation applications, and so use of the waveform information for this purpose is still in the early stages but is potentially very promising (Disney et al. 2014). Field intercomparisons are being used to test the various strengths and weaknesses of the different instrument approaches (Armston et al. 2013b).

A key obstacle of using TLS for 3D structure is transforming point cloud data into some form of topologically-structured description of individual trees, preferably in a robust, automated way. Estimating tree diameter at breast height and stem number-density is fairly easy; height can be straightforward but requires points to be returned from the top of the canopy, which can be problematic in tall, dense canopies. Topology is much harder, as it requires an association between points and organs within a particular tree (branches, leaves). Various 3D tree reconstruction methods have been proposed for TLS data (e.g. Gorte and Pfeifer 2004). Limitations of these methods have been the speed and the requirement for a large number of heuristic thresholds. Recent work has shown that development of more robust and rapid methods is possible (Raumonen et al. 2013).

An additional problem for any reconstruction method is validation, given the practical difficulty of measuring 3D structure for other than the simplest trees. Detailed 3D radiative transfer models as described above are proving one possible route for overcoming this limitation (Disney et al. 2012). In turn, the resulting tree reconstructions open the way for routine development of 3D scene models for remote sensing simulations. Figure 11.9 shows an example of a single TLS scan collected in an Australian *Eucalyptus* forest. The rich structural nature of the data is immediately apparent. Also shown are lidar 'hits' from a single tree extracted from the resulting point cloud, and a 3D reconstruction of the same tree via the method of Raumonen et al. (2013). It is worth noting that other uses of TLS are in estimating canopy clumping and gap fraction from the ground. TLS is potentially a more accurate way to estimate clumping than e.g. hemiphoto methods, as the effective resolution is generally higher, and few if any assumptions are required to estimate gap fraction (Casella et al. 2013). Reconstruction of tree volume from TLS data allows rapid, accurate and non-destructive estimates of above ground biomass to be made (Calders et al. 2014). The TLS measurement errors are also independent of tree size, unlike biomass estimates inferred indirectly from tree height or diameter measurements.

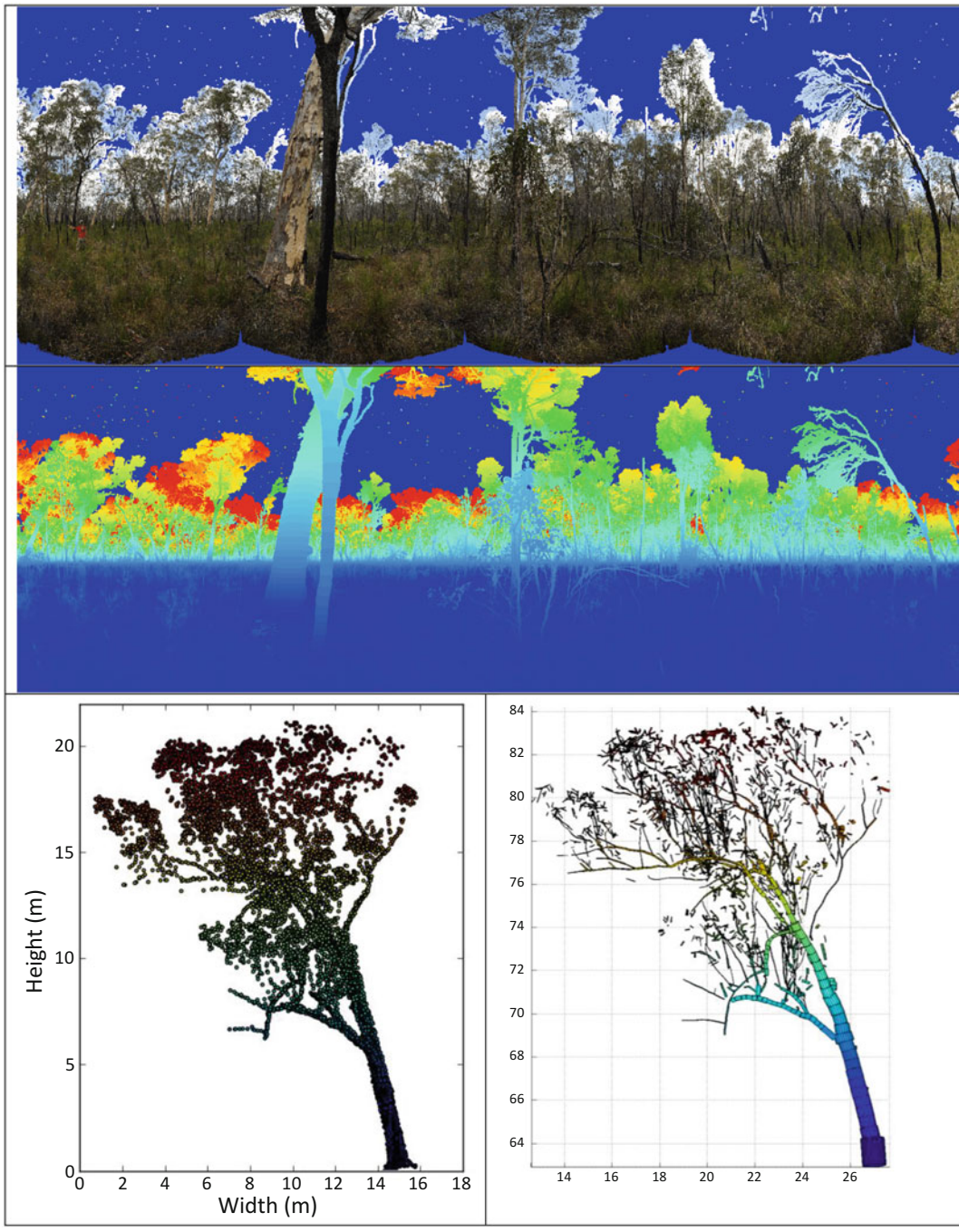


*Fig. 11.9.* Examples of Riegl VZ-400 terrestrial laser scanning (TLS) data from a bush site in Queensland, Australia and 3D tree structure reconstructed from the resulting scans. *Top*: 360° panorama of individual hemispheric photographs taken from a camera mounted on the TLS instrument. *Centre*: TLS scan, with height mapped to color. *Bottom left*: TLS points from a single tree extracted from the point cloud data (*color* represents height above the ground); *bottom right*: 3D reconstruction of the same tree (*color* again represents height) using the method of Raumonen et al. (2013)

### 5. RADAR Systems

RADAR is an alternative promising instrument for canopy structure and function observations (Lee and Pottier 2009). In fact, RADAR has the specific, very great, advantage over optical reflected methods of all-weather operation. Longer wavelength (tens of cm) RADAR is potentially sensitive to much higher levels of biomass due to penetration through the upper canopy and interacting only with larger trunks and branches. Unlike lidar systems, scanning imaging RADAR systems are well-advanced from an engineering perspective, allowing for the wide area coverage that is often such an advantage of remote sensing. High-resolution interferometric synthetic aperture RADAR (InSAR) instruments also hold promise for measurements of canopy height and structure (Krieger et al. 2007). However, the radiative transfer problem in the RADAR domain is less well-understood than for optical wavelengths due to complications as a result of phase, polarization and coherence. As a result, exploitation of RADAR for vegetation applications has been primarily via empirical relationships between backscatter and amount/biomass. Yet, these measurements are known to have significant shortcomings in terms of their ability to reliably predict biomass as a function of backscatter. This arises in part due to gaps in understanding of the physical processes governing the observed backscatter (Mitchard et al. 2011; Woodhouse et al. 2012).

## B. Fluorescence and Canopy Function

Plant physiological stress studies mainly focus on pulse-modulated chlorophyll fluorescence, but the light levels needed for saturated pulses are far too high such that this method is not practical for EO (Schreiber et al. 1995; Baker 2008). As a potential alternative, there has been major interest in solar-induced chlorophyll fluorescence ($F_s$). $F_s$ results from the excitation of chlorophyll molecules within assimilating leaves in the canopy and it is produced at the core of Photosystems I and II, primarily at photosystem II. Chlorophyll fluorescence is the remaining part of intercepted light energy, typically less than a few percent, that is not used photochemically nor dissipated non-photochemically. Fluorescence occurs at longer wavelengths than the excitation light wavelength (typically 650–800 nm for sunlight). Although minor, $F_s$ is often inversely related to photosynthesis, except when non-photochemical quenching of fluorescence occurs. Under stress, or in conditions where irradiance exceeds that required for photosynthesis, plant tissues increase heat production to dissipate excess energy. This tends to decrease $F_s$, at least initially. Therefore, the resulting level of $F_s$ is a balance between the radiation used for photosynthesis, heat production, and chlorophyll fluorescence. Steady-state measurements of $F_s$ are therefore highly responsive to changes in environmental conditions and can be used as a near-direct indicator of plant photosynthetic function (Moya et al. 2004; Guanter et al. 2012, 2014).

This rapid response of $F_s$ to changing environment (temperature, light) and canopy state (water, internal temperature, nutrients etc.) has elicited significant interest in the possibility of relating remotely sensed measurements of $F_s$ to canopy function and stress in particular. However, the induced fluorescence signal is only 1–5 % of the total reflected solar signal in the NIR, making it difficult to separate from the background reflected signal (Meroni et al. 2009). Malenovsky et al. (2009) review some of the challenges of measuring $F_s$ from the solar reflected signal. Despite these issues, there have been several attempts to employ these measurements, including the ESA FLEX (Fluorescence Explorer) mission, primarily based on using narrow, specific dark lines of the solar and atmospheric spectrum in which irradiance is strongly reduced (the so-called Fraunhofer lines). Three main Fraunhofer features have been exploited for $F_s$ estimation: Hα due to

hydrogen (H) absorption (centred at 656.4 nm) and two telluric oxygen ($O_2$) absorption bands O2-B (687.0 nm) and O2-A (760.4 nm). These lead to variants of the so-called Fraunhofer Line Depth (FLD) methods, in which $F_s$ is estimated from some form of ratio of the measured signal in a Fraunhofer band to that measured in a reference band just outside the Fraunhofer band (see Meroni et al. 2009 for details of these methods). Key limitations for spaceborne applications include the requirement for very accurate spectral calibration, and the removal of atmospheric and directional effects. However, a major advantage of exploiting existing (and future) imaging spectroradiometers is that they have become relatively common and acquire spatial image data over wide areas. Guanter et al. (2007) demonstrated that $F_s$ retrieval was possible from the MERIS sensor aboard ESA's Envisat platform. Their approach incorporated $F_s$ retrieval into an atmospheric radiative transfer scheme so that $F_s$ and surface reflectance were retrieved consistently from measured at-sensor radiance. This holds the promise for more systematic retrievals from newer sensors such as ESA's Sentintel 5 precursor mission, due for launch in 2015 (http://esamultimedia.esa.int/docs/S5-prec_Data_Sheet.pdf).

A new approach to retrieve $F_s$ was recently developed that does not rely on the reflected solar signal, but uses estimates of changes in the depth of solar Fraunhofer lines, which tend to decrease due to in-filling by $F_s$ (Joiner et al. 2011; Frankenberg et al. 2011a, b). These methods rely on high spectral resolution observations in the 755–775 nm range, which can resolve individual Fraunhofer lines overlapping with the $F_s$ emission region. A key advantage of this method is that Fraunhofer line depth is unaffected by atmospheric scattering and absorption in certain narrow spectral windows. If these windows can be observed, then it is possible to estimate the in-filling due to $F_s$ emission, which can of course only arise from vegetation. Such an approach has only become feasible since the launch of the Japanese Greenhouse Gases Observing SATellite "IBUKI" (GOSAT), carrying the Thermal and Near infrared Sensor for carbon Observation (TANSO) (http://www.gosat.nies.go.jp/index_e.html). The TANSO Fourier Transform Spectrometer (FTS) was designed for measuring column-averaged atmospheric $CO_2$ on global scales. The possibility for retrieving $F_s$ was a serendipitous after-thought. TANSO-FTS observations are by no means ideal for $F_s$ due to their large spatial extent (tens km footprint), and limited spatial and temporal coverage due to the instrument design. Despite these issues, the first retrievals of $F_s$ have shown large-scale patterns consistent with expectations of seasonal and regional variations in productivity (Joiner et al. 2011). An example global map of $F_s$ derived from TANSO-FTS data is shown in Fig. 11.10.

The results suggest that estimates of $F_s$ correlate strongly with independent estimates of GPP (Frankenberg et al. 2011b; Guanter et al. 2012, 2014). Critically, $F_s$ also seems to contain information which is independent of standard satellite reflectance-derived estimates of productivity via NDVI or EVI, for example, that basically measure vegetation 'greenness' i.e. some property related to vegetation amount. In addition, the $F_s$ signal is likely to be much more sensitive to canopy stress due to its origins in the photosynthetic machinery. This might allow exploration of large-scale impacts of stressors on vegetation productivity. As an example of this, Lee et al. (2013) used satellite fluorescence to show that instantaneous midday productivity (GPP) was reduced by as much as 15 % across the Amazon due to severe drought conditions in 2010. This interest in fluorescence as an indicator of GPP has led to new ways to exploit data from sensors primarily aimed at atmospheric trace gas applications. Joiner et al. (2013) have extracted fluorescence from the Japanese GOME-2 instrument, at higher precision and over smaller spatial and temporal scales than is possible with

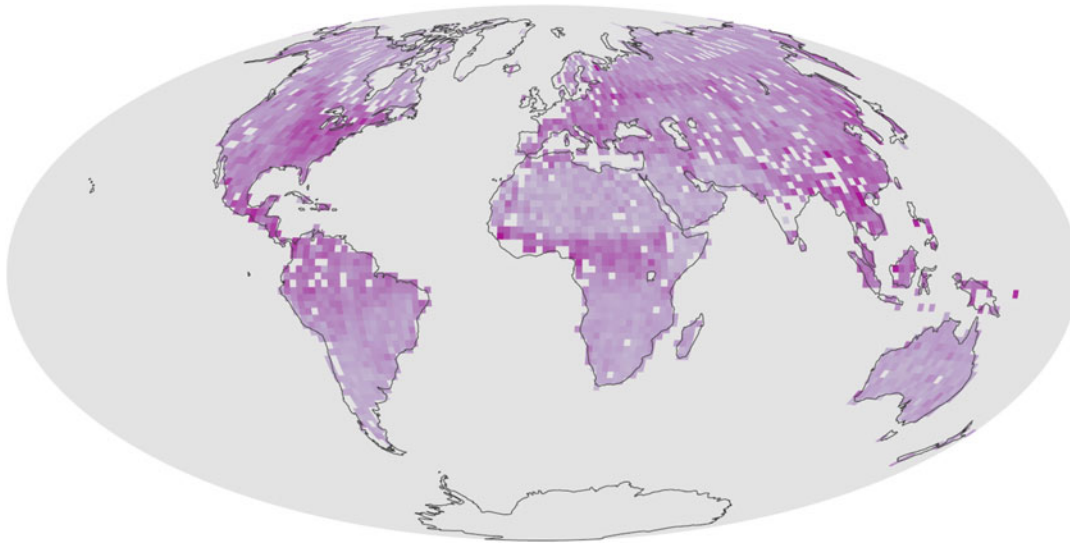

*Fig. 11.10.* Sun-induced steady-state fluorescence yield ($F_s$) estimated from GOSAT TANSO-FTS observations composited during July 2009. Color intensity represents intensity of $F_s$ in arbitrary units. Image from NASA Earth Observatory, created by Robert Simmon, using data from GOSAT (http://visibleearth.nasa.gov/view.php?id=51121)

GOSAT. This work holds the promise of more detailed maps of fluorescence from space in the near future, which has in turn led to an increase in interest as to how to understand and exploit this signal using models.

The intriguing and unique information content of $F_s$ has led to work on modelling the signal at the leaf and canopy levels in order to understand the signal and potentially allow parameter retrievals (Miller et al. 2005). $F_s$ models rely on embedding a model of leaf-level fluorescence within a canopy reflectance model. The FLSAIL model (Rosema et al. 1991) was an extension of the SAIL canopy reflectance model (Verhoef 1984) with $F_s$ contributions modelled through a doubling method. The model was primarily developed for describing laser-induced rather than solar-induced fluorescence. Olioso et al. (1992) used a simple Beer's Law approximation for canopy and leaf-level extinction and allowed for within-canopy gradient in chlorophyll content to account for variations in leaf biochemistry. The 3D DART model has also been modified to provide estimates of fluorescence at the canopy level (Miller et al. 2005). FlurMODleaf is perhaps the most sophisticated $F_s$ model, based on the PROSPECT model described above (Miller et al. 2005; Zarco-Tejada et al. 2006). This model has been used in various studies to show the influence of fluorescence on hyperspectral reflectance data (Zarco-Tejada et al. 2006, 2009; Middleton et al. 2008).

Reliable remotely-sensed observations of fluorescence are still in their infancy but they hold out the tantalising prospect of much more direct estimates of canopy function, productivity, and stress than at present, from spaceborne instruments based on visible and near infra-red radiation reflectance (Grace et al. 2007). NASA's Orbiting Carbon Observatory 2 (launched in mid-2014) may be capable of retrieving $F_s$ from solar reflected signal, and there is increasing interest in other ways to retrieve $F_s$ and vegetation productivity from both spaceborne and airborne hyperspectral data.

## V. Conclusions

Various issues arise in using remote sensing in estimating vegetation structure and function in a quantitative sense. The primary limitation clearly is the indirect nature of most remote sensing measurements. However, there are also great capabilities that now exist for mapping, even indirectly, canopy state and function over wide areas and with repeated sampling, allowing for studies of phenology, disturbance and anthropogenic impacts. We have explored the key role that vegetation structure plays in providing a link between incoming radiation and how this radiation is subsequently scattered or absorbed within the canopy before exiting to provide the remote sensing signal. New developments in understanding and modelling the fundamental nature of these interactions are allowing us to chart a route from measurements made at the top-of-the atmosphere to estimates of canopy state and function. These developments are allowing us to unpick the relationships between 'effective' canopy parameters, simplified or approximate manifestations of measurable physical parameters, and their real measurable counterparts. Effective parameters allow us to model the radiation signal in practical, rapid models that are required to operate on global scales. The effective nature of the parameters, however, makes such models difficult to test and validate. Increases in the resolution and physical accuracy of large-scale land surface models has highlighted these discrepancies, but also calls for improvements in representations of vegetation. This is critical to reducing uncertainty in modelling the responses of terrestrial vegetation to changes in climate and land use, particularly via the terrestrial carbon cycle.

A range of new remote sensing measurements providing more direct information on canopy structure and function have been discussed. Terrestrial and airborne lidar systems, notably full-waveform and multispectral, are providing new information on canopy structure. Observations of canopy fluorescence have provided promising estimates of canopy function, particularly under stress. These new observations are being exploited through developments in detailed 3D canopy and leaf models, which are making use of the continued increases in computing power to reduce the requirements for approximations.

From 2000 on there has been an unprecedented increase in high quality calibrated consistent and error-quantified satellite measurements of terrestrial vegetation at resolutions of 250 m – 1 km, covering the globe every few days. Notwithstanding limitations, these observations are now central to a huge range of applications. Indeed, many of these observations have been identified as so-called 'essential climate variables' (http://www.wmo.int/pages/prog/gcos/index.php?name=EssentialClimateVariables).

However, the future is perhaps a little more uncertain: current activities by major space agencies include plans for continuation of many, but not all, of the existing observations of the land surface that have proved so useful. Some of these new systems will provide observations with reduced capability and/or scope than their predecessors, for a variety of practical reasons. Given what we have, and what is to come, we should look forward to the coming decade as one that will likely provide as many developments in our ability to measure and understand terrestrial vegetation as the last decade undoubtedly had.

## Acknowledgments

I acknowledge the support of UCL Geography and the NERC National Centre for Earth Observation (NCEO), as well as the University of Queensland for hosting me during some of this work. I also acknowledge various colleagues for the numerous and varied discussions over the last few years, that have led to thoughts and collaborations on issues

discussed here, including (inter alia): P Lewis, J Gomez-Dans, MJ Disney, M Barnsley, T Quaife, M DeKauwe, S Hancock, M Williams, S Quegan C Schaaf, A Strahler, Y Knyazkhin, B Pinty, JL Widlowski, J Armston and K Calders among many others. I am grateful to Prof. Vince Gutschick and the Mathematical Biosciences Institute of Ohio State University, for the invitation to the MBI Workshop on Modelling Plant Development which provided initial impetus for this work.

## References

Allen WA, Gausman HW, Richardson AJ, Thomas JR (1969) Interaction of isotropic light with a compact plant leaf. J Opt Soc Am 59:1376–1379

Allen WA, Gausman HW, Richardson AJ (1970) Mean effective optical constants of cotton leaves. J Opt Soc Am 60:542–547

Alton PB, North PRJ, Los SO (2007) The impact of diffuse sunlight on canopy light-use efficiency, gross photosynthetic product and net ecosystem exchange in three forest biomes. Glob Chang Biol 13:776–787

Angert A, Biraud S, Henning CC, Bauermann W, Pinzon J, Tucker CJ, Fung I (2005) Drier summers cancel out the $CO_2$ uptake enhancement induced by warmer springs. Proc Natl Acad Sci U S A 102:10823–10827

Armston J, Disney MI, Lewis P, Scarth P, Phinn S, Lucas R, Bunting P, Goodwin N (2013a) Direct retrieval of canopy gap probability using airborne waveform lidar. Remote Sens Environ 134:24–38

Armston J, Newnham G, Strahler AH, Schaaf C, Danson M, Gaulton R, Zhang Z, . . ., Wu S (2013b) Intercomparison of terrestrial laser scanning instruments for assessing forested ecosystems: a Brisbane field experiment, B11G-0443, In: Proc. AGU San Francisco, Dec. 2013 http://128.197.168.195/wp-content/uploads/2013/11/Armston_Brisbane.pdf

Asner GP, Mascaro J (2014) Mapping tropical forest carbon: Calibrating plot estimates to a simple LiDAR metric. Remote Sens Environ 140:614–624

Asner GP, Powell GV, Mascaro J, Knapp DE, Clark JK, Jacobson J, Kennedy-Bowdoin T, . . ., Hughes RF (2010) High resolution forest carbon stocks and emissions in the Amazon. Proc Natl Acad Sci USA 107:16738–16742

Asrar G (ed) (1989) Theory and Applications of Optical Remote Sensing. Wiley, New York

Baccini A, Goetz SJ, Walker WS, Laporte NT, Sun M, Sulla-Menashe D, Hackler J, . . ., Houghton RA (2012) Estimated carbon dioxide emissions from tropical deforestation improved by carbon-density maps. Nat Clim Change 2:182–185

Baker, Neil R. "Chlorophyll fluorescence: a probe of photosynthesis in vivo."Annu. Rev. Plant Biol. 59 (2008): 89–113

Baranoski GVG (2006) Modeling the interaction of infrared radiation (750 to 2500 nm) with bifacial and unifacial plant leaves. Remote Sens Environ 100:335–347

Best MJ, Pryor M, Clark DB, Rooney GG, Essery RLH, Ménard CB, Edwards JM, . . ., Harding RJ (2011) The Joint UK Land Environment Simulator (JULES), model description – Part 1: Energy and water fluxes. Geosci Model Dev 4:677–699

Brando P, Goetz S, Baccini A, Nepstad DC, Beck PSA, Chiristman MC (2010) Seasonal and interannual variability of climate and vegetation indices across the Amazon. Proc Natl Acad Sci U S A 107:14685–14690

Brodersen CR, Voglemann TC, Williams WE, Gorton H (2008) A new paradigm in leaf-level photosynthesis: direct and diffuse lights are not equal. Plant Cell Environ 31:159–164

Bunnik NJJ (1978) The multispectral reflectance of shortwave radiation of agricultural crops in relation with their morphological and optical properties. PhD Thesis, In Mededelingen Landbouwhogeschool, Wageningen University, Wageningen

Brut A, Rüdiger C, Lafont S, Roujean J-L, Calvet J-C, Jarlan L, Gibelin A-L, . . ., Ceschis E (2009) Modelling LAI at a regional scale with ISBA-A-gs: comparison with satellite-derived LAI over southwestern France. Biogeosciences 6:1389–1404

Calders K, Newnham G, Burt A, Murphy S, Raumonen P, Herold M, Culvenor D, . . ., Kaasalainen M (2014) Non-destructive estimates of above-ground biomass using terrestrial laser scanning. Methods Ecol Evol, in press. doi: 10.1111/2041-210X.12301

Campbell GS (1986) Extinction coefficient for radiation in plant canopies calculated using an ellipsoidal inclination angle distribution. Agric For Meteorol 36:317–321

Carrer D, Roujean JL, Lafont S, Boone A, Calvet, JC (2012) A vegetation radiative transfer scheme in ISBA-A-gs interactive vegetation model. In: Proceedings of IGARSS2012. Munich, Germany, 22–27 July 2012, pp 1151–1154

Casella E, Disney MI, McKay H (2013) tLiDAR methodologies can overcome limitations in

estimating forest canopy LAI from conventional hemispherical photograph analyses. In: Proceedings of Functional Structural Plant Modelling 2013 (FSPM2013), Saariselkä, Finland, 9–14 June, 2013

Cescatti A, Niinemets Ü (2004) Leaf to landscape. In: Smith WK, Vogelmann TC, Critchley C (eds) Ecological Studies: Photosynthetic Adaptation, vol 178. Springer, New York, pp 42–85

Chandrasekhar S (1960) Radiative Transfer. Dover, New York

Chapin FS III, Chapin MC, Matson PA, Vitousek P (2011) Principles of Terrestrial Ecosystem Ecology, 2nd edn. Springer, New York

Combes D, Bousquet L, Jacquemoud S, Sinoquet H, Varlet-Grancher C, Moya I (2007) A new spectrogoniophotometer to measure leaf spectral and directional optical properties. Remote Sens Environ 109:107–117

Danson FM, Gaulton R, Armitage RP, Disney MI, Gunawan O, Lewis PE, Pearson G, Ramirez AF (2014) Developing a dual-wavelength full-waveform terrestrial laser scanner to characterise forest canopy structure. Agric For Meteorol 198–199:7–14

Dawson TP, Curran PJ, Plummer SE (1998) LIBERTY – modeling the effects of leaf biochemical concentration on reflectance spectra. Remote Sens Environ 65:50–60

Denman KL, Brasseur G, Chidthaisong A, Ciais P, Cox PM, Dickinson RE, Hauglustaine D, . . ., Zhang X (2007) Couplings between changes in the climate system and biogeochemistry. In: Solomon S, Qin D, Manning M, Chen Z, Marquis M, Averyt KB, Tignor M, Miller HL (eds) Climate Change 2007: The Physical Science Basis. Contribution of Working Group I to the Fourth Assessment Report of the Intergovernmental Panel on Climate Change. Cambridge University Press, Cambridge, pp 499–587

Dickinson RE (1983) Land surface processes and climate—surface albedos and energy balance. Adv Geophys 25:305–353

Disney MI, Lewis P, North P (2000) Monte Carlo ray tracing in optical canopy reflectance modelling. Remote Sens Rev 18:163–197

Disney MI, Lewis P, Quaife T, Nichol, C (2005) A spectral invariant approach to modeling canopy and leaf scattering. In: Proceedings of the 9th International Symposium on Physical Measurements and Signatures in Remote Sensing (ISPMSRS), 17–-19 October 2005, Beijing, China, Part 1: 318–320

Disney MI, Lewis P, Saich P (2006) 3D modelling of forest canopy structure for remote sensing simulations in the optical and microwave domains. Remote Sens Environ 100:114–132

Disney MI, Lewis P, Bouvet M, Prieto-Blanco A, Hancock S (2009) Quantifying surface reflectivity for spaceborne lidar via two independent methods. IEEE Trans Geosci Remote Sens 47:3262–3271

Disney MI, Kalogirou V, Lewis PE, Prieto-Blanco A, Hancock S, Pfeifer M (2010) Simulating the impact of discrete-return lidar system and survey characteristics over 2 young conifer and broadleaf forests. Remote Sens Environ 114:1546–1560

Disney MI, Lewis P, Gomez-Dans J, Roy D, Wooster M, Lajas D (2011) 3D radiative transfer modelling of fire impacts on a two-layer savanna system. Remote Sens Environ 115:1866–1881

Disney MI, Lewis P, Raumonen P (2012) Testing a new vegetation structure retrieval algorithm from terrestrial lidar scanner data using 3D models. In: Proceedings of Silvilaser 2012, Vancouver, BC, Canada, 16–19 September 2012

Disney MI, Burt A, Calders K, Raumonen P, Gonzalez de Tanago J, Cuni Sanchez A, Herold M, Armston J, Lewis S, Lines S, Lewis P (2014) New applications of 3D measurements and modelling to quantifying forest structure and biomass. In: Global Vegetation Modelling and Measurement (GV2M) meeting, Avignon, France, 3–7 Feb 2014

Douglas ES, Strahler AH, Martel J, Cook T, Mendillo C , Marshall R, Chakrabarti S, . . ., Lovell J (2012) DWEL: a dual-wavelength Echidna lidar for ground-based forest scanning. In: Proceedings of IGARSS2012, 22–27 July 2012, Munich, Germany, pp 4998–5001

Dubayah RO, Drake JB (2000) Lidar remote sensing for forestry. J For 98:44–46

Dubayah RO, Sheldon SL, Clark DB, Hofton MA, Blair JB, Hurtt GC et al (2010) Estimation of tropical forest height and biomass dynamics using lidar remote sensing at La Selva, Costa Rica. J Geophys Res 115

España M, Baret F, Aries F, Andrieu B, Chelle M (1999) Radiative transfer sensitivity to the accuracy of canopy structure description. The case of a maize canopy. Agronomie 19:241–254

Feret JB, François C, Asner GP, Gitelson AA, Martin RE, Bidel LPR, Ustin SL, le Maire G, Jacquemoud S (2008) PROSPECT-4 and 5: advances in the leaf optical properties model separating photosynthetic pigments. Remote Sens Environ 112:3030–3043

Flerchinger GN, Yu Q (2007) Simplified expressions for radiation scattering in canopies with ellipsoidal leaf angle distributions. Agric For Meteorol 144:230–235

Frankenberg C, Butz A, Toon GC (2011a) Disentangling chlorophyll fluorescence from

atmospheric scattering effects in O2A-band spectra of reflected sun-light. Geophys Res Lett 38, L03801

Frankenberg C, Fisher JB, Worden J, Badgley G, Saatchi SS, Lee J-E, Toon GC, . . ., Yokota T (2011b) New global observations of the terrestrial carbon cycle from GOSAT: Patterns of plant fluorescence with gross primary productivity. Geophys Res Lett 38:L17706

Fung AK (1994) Microwave Scattering and Emission Models and Their Applications. Artech House, Norwood

Ganguly S, Schull MA, Samanta A, Shabanov NV, Milesi C, Nemani R, Knyazikhin YV, Myneni RB (2008) Generating vegetation leaf area index earth system data records from multiple sensors. Part 1: Theory. Remote Sens Environ 112:4333–4343

Ganguly S, Nemani R, Zhong G, Hashimoto H, Milesi C, Michaelis M, Wang W, . . ., Myneni RB (2012) Generating global leaf area index from Landsat: algorithm formulation and demonstration. Remote Sens Environ 122:185–202

Gastellu-Etchegorry JP, Martin E, Gascon F (2004) Dart: a 3D model for simulating satellite images and studying surface radiation budget. Int J Remote Sens 25:73–96

Godin C, Sinoquet H (2005) Functional–structural plant modelling. New Phytol 166:705–708

Goel NS (1988) Models of vegetation canopy reflectance and their use in the estimation of biophysical parameters from reflectance data. Remote Sens Rev 4:1–222

Goel NS, Strebel DE (1984) Simple beta distribution representation of leaf orientation in vegetation canopies. Agron J 75:800–802

Goel NS, Thompson RL (2000) A snapshot of canopy reflectance models, and a universal model for the radiation regime. Remote Sens Rev 18:197–225

Gorte B, Pfeifer N (2004) Structuring laser-scanned trees using 3D mathematical morphology. Int Arch Photogramm Remote Sens XXXV:929–933

Govaerts YM (1996) A model of light scattering in three-dimensional plant canopies: a Monte Carlo ray tracing approach. Office for Official Publication of the European Communities

Govaerts Y, Verstraete MM (1998) Raytran: a Monte Carlo ray-tracing model to compute light scattering in three-dimensional heterogeneous media. IEEE Trans Geosci Remote Sens 36:493–505

Grace J, Nichol C, Disney MI, Lewis P, Quaife T, Bowyer P (2007) Can we measure photosynthesis from space? Glob Chang Biol 13:1484–1497

Guanter L, Alonso L, Gomez-Chova L, Amoros-Lopez J, Moreno J (2007) Estimation of solar-induced vegetation fluorescence from space measurements. Geophys Res Lett 34:L08401

Guanter L, Frankenberg C, Dudhia A, Lewis PE, Gomez-Dans J, Kuze A, Suto H, Grainger RG (2012) Retrieval and global assessment of terrestrial chlorophyll fluorescence from GOSAT space measurements. Remote Sens Environ 121:236–257

Guanter L, Zhang Y, Jung M, Joiner J, Voigt M, Berry JA, Frankenberg C, . . ., Griffis TJ (2014) Global and time-resolved monitoring of crop photosynthesis with chlorophyll fluorescence. Proc Natl Acad Sci USA 111:E1327–E1333

Hapke B (1981) Bidirectional reflectance spectroscopy. I. Theory. J Geophys Res 86:3039–3054

Harding DJ, Carabajal CC (2005) ICESat waveform measurements of within-footprint topographic relief and vegetation vertical structure. Geophys Res Lett 32, L21S10

Henderson-Sellers A, Irannejad P, McGuffie K, Pitman A (2003) Predicting land-surface climates: better skill or moving targets? Geophys Res Lett 30:1777

Hosgood B, Jacquemoud S, Andreoli G, Verdebout J, Pedrini G, Schmuck G (1995) LOPEX: Leaf optical properties experiment 93. Technical Report EUR 16095 EN, Joint Research Center, European Commission, Institute for Remote Sensing Applications

Houser P, De Lannoy G, Walker JP (2012) Hydrologic data assimilation. In: Tiefenbacher JP (ed) Approaches to Managing Disaster – Assessing Hazards, Emergencies and Disaster Impacts. InTech, Rijeka, 162 p

Huang D, Knyazikhin Y, Dickinson R, Rautiainen M, Stenberg P, Disney MI, Lewis P, . . ., Myneni RB (2007) Canopy spectral invariants for remote sensing and model applications. Remote Sens Environ 106:106–122

Hyyppä J, Hyyppä H, Leckie D, Gougeonm F, Yu X, Maltamo M (2008) Review of methods of small-footprint airborne laser scanning for extracting forest inventory data in boreal forests. Int J Remote Sens 29:1339–1366

Jacquemoud S, Ustin S (2008) Modelling leaf optical properties. Photobiological Sciences Online (Smith KC , ed.) American Society for Photobiology, http://www.photobiology.info/

Jacquemoud S, Ustin SL, Verdebout J, Schmuck G, Andreoli G, Hosgood B (1996) Estimating leaf biochemistry using the PROSPECT leaf optical properties model. Remote Sens Environ 56:194–202

Jacquemoud S, Verhoef W, Baret F, Bacour C, Zarco-Tejada PJ, Asner GP, Francois C, Ustin SL (2009) PROSPECT + SAIL Models: a review of use for vegetation characterization. Remote Sens Environ 113:56–66

Joiner J, Yoshida Y, Vasilkov AP, Yoshida Y, Corp LA, Middleton EM (2011) First observations of global and seasonal terrestrial chlorophyll fluorescence from space. Biogeosciences 8:637–651

Joiner J, Guanter L, Lindstrot R, Voigt M, Vasilkov AP, Middleton EM, Huemmerich KF, . . ., Franenberg C (2013) Global monitoring of terrestrial chlorophyll fluorescence from moderate spectral resolution near-infrared satellite measurements: methodology, simulations and application to GOME-2. Atmos Meas Tech Discuss 6:3883–3930

Jones HG (2014) Plants and Microclimate: A Quantitative Approach to Environmental Plant Physiology, 3rd edn. CUP, Cambridge

Jones HG, Vaughan RA (2010) Remote Sensing of Vegetation: Principles, Techniques and Applications. OUP, Oxford

Knorr W, Heimann M (2001) Uncertainties in global terrestrial biosphere modeling: 1. A comprehensive sensitivity analysis with a new photosynthesis and energy balance scheme. Glob Biogeochem Cycles 15.1:207–225

Knorr W, Kaminski T, Scholze M, Gobron N, Pinty B, Giering R, Mathieu P-P (2010) Carbon cycle data assimilation with a generic phenology model. J Geophys Res 115, doi:10.1029/2009JG001119

Knyazikhin YV, Marshak AL, Myneni RB (1992) Interaction of photons in a canopy of finite dimensional leaves. Remote Sens Environ 39:61–74

Knyazikhin YV, Kranigk J, Myneni RB, Panfyorov O, Gravenhorst G (1998) Influence of small-scale structure on radiative transfer and photosynthesis in vegetation canopies. J Geophys Res 103:6133–6144

Knyazikhin YV, Schull MA, Liang X, Myneni RB, Samanta A (2011) Canopy spectral invariants. Part 1: A new concept in remote sensing of vegetation. J Quant Spectrosc Radiat Transf 112:727–735

Knyazikhin YV, Schull MA, Stenberg P, Mõttus M, Rautiainen M, Yang Y, Marshak A, . . ., Myneni RB (2013) Hyperspectral remote sensing of foliar nitrogen content. Proc Natl Acad Sci USA 110: E185–E192

Krieger G, Moreira A, Fiedler H, Hajnsek I, Werner M, Younis M, Zink M (2007) TanDEM-X: A satellite formation for high-resolution SAR interferometry. IEEE Trans Geosci Remote Sens 45:3317–3341

Kubelka P, Munk F (1931) Zeit Für Tekn Physik 12:593

Lafont S, Zhao Y, Calvet J-C, Peylin P, Ciais P, Maignan F, Weiss M (2012) Modelling LAI, surface water and carbon fluxes at high-resolution over France: comparison of ISBA-A-gs and ORCHIDEE. Biogeosciences 9:439–456

Lee J-S, Pottier E (2009) Polarimetric radar imaging: from basics to applications. CRC Press, Boca Raton

Lee J-E, Franksnberg C, van der Tol C, Berry JA, Guanter L, Boyce CK, Fisher JB, . . ., Saatchi, S (2013) Forest productivity and water stress across Amazonia: observations from GOSAT chlorophyll fluorescence. Proc Royal Soc B 280:1471–2954

Leersnijder RP (1992) PINOGRAM: A Pine Growth Area Model. WAU dissertation 1499, Wageningen Agricultural University, The Netherlands

Lefsky MA, Cohen WB, Parker GG, Harding DJ (2002) Lidar remote sensing for ecosystem studies. Biogeosciences 52:19–30

Lefsky MA, Harding DJ, Keller M, Cohen WB, Carabajal CC, Espirito-Santo FDB, Hunter MO, de Oliveira R Jr (2005) Estimates of forest canopy height and aboveground biomass using ICESat. Geophys Res Lett 32:L22S02

Lewis P (1999) Three-dimensional plant modelling for remote sensing simulation studies using the Botanical Plant Modelling System (BPMS). Agron Agric Environ 19:185–210

Lewis P, Disney MI (1998) The botanical plant modeling system (BPMS): a case study of multiple scattering in a barley canopy. In: Proceedings of IGARSS'98, Seattle, USA.

Lewis P, Disney MI (2007) Spectral invariants and scattering across multiple scales from within-leaf to canopy. Remote Sens Environ 109:196–206

Lewis P, Gómez-Dans J, Kaminski T, Settle J, Quaife T, Gobron N, Styles J, Berger M (2012) An Earth Observation Land Data Assimilation System (EO-LDAS). Remote Sens Environ 120:219–235

Liang S (2004) Quantitative Remote Sensing of Land Surfaces. Wiley, New York

Lynch C (2008) Big data: How do your data grow? Nature 455:28–29

Maas HG, Bientert A, Scheller S, Keane E (2008) Automatic forest inventory parameter determined from terrestrial laser scanner data. Int J Remote Sens 29:1579–1593

Malenovsky Z, Mishra KB, Zemek F, Rascher U, Nedbal L (2009) Scientific and technical challenges in remote sensing of plant canopy reflectance and fluorescence. J Exp Bot 60:2987–3004

Mallet C, Bretar F (2009) Full-waveform topographic lidar: state-of-the-art. ISPRS J Photogramm Remote Sens 64:1–16

Marshak A, Knyazikhin YV, Chiu JC, Wiscombe WJ (2011) Spectrally invariant approximation within atmospheric radiative transfer. J Atmos Sci 68:3094–3111

Martin G, Josserand SA, Bornman JF, Vogelmann TC (1989) Epidermal focussing and the light microenvironment within leaves of Medicago sativa. Physiol Plant 76:485–492

Meador I, Weaver WR (1980) Two-stream approximations to radiative transfer in planetary atmospheres: a unified description of existing methods and new improvements. J Atmos Sci 37:630–643

Mêch R, Prusinkiewicz P (1996) Visual models of plants interacting with their environment. Proceedings of SIGGRAPH 96. New Orleans, Louisiana, August 4–9 1996. In computer graphics proceedings, annual conference series, ACM SIGGRAPH, pp 397–410

Melamed NT (1963) Optical properties of powders. Part I. Optical absorption coefficients and the absolute value of the diffuse reflectance. Part II. Properties of luminescent powders. J Appl Phys 34:560–570

Mercado LM, Bellouin NM, Sitch S, Boucher O, Huntingford C, Wild M, Cox PM (2009) Impact of changes in diffuse radiation on the global land carbon sink. Nature 458:1014–1018

Meroni M et al (2009) Remote sensing of solar-induced chlorophyll fluorescence: review of methods and applications. Remote Sens Environ 113(10):2037–2051

Middleton E, Corp LA, Campbell PKE (2008) Comparison of measurements and FluorMOD simulations for solar-induced chlorophyll fluorescence and reflectance of a corn crop under nitrogen treatments. Int J Remote Sens 29:5193–5213

Miller J, Berger M, Goulas Y, Jacquemoud S, Louis J, Mohammed G, Moise N, . . ., Zarco-Tejada P (2005) Development of a vegetation fluorescence canopy model, ESTEC Contract No. 16365/02/NL/FF Final Report

Mitchard ETA, Saatchi SS, Woodhouse IR, Feldpausch TR, Lewis SL, Sonké B, Rowland C, Meir P (2011) Measuring biomass changes due to woody encroachment and deforestation/degradation in a forest-savanna boundary region of central Africa using multi-temporal L-band radar backscatter. Remote Sens Environ 115:2861–2873

Monsi M, Saeki T (1953) Über den Lichtfaktor in den Pflanzengesellscahften und seine Bedeutung für die Stoffproduktion. Jpn J Bot 14:22–52. *Translated as*: Monsi M, Saeki T (2005) On the factor light in plant communities and its importance for matter production. Ann Bot 95:549–567

Monteith JL, Unsworth MH (2008) Principles of Environmental Physics, 3rd edn. Academic, Burlington

Morsdorf F, Nichol C, Malthus T, Woodhouse IH (2009) Assessing forest structural and physiological information content of multi-spectral LiDAR waveforms by radiative transfer modelling. Remote Sens Environ 113:2152–2163

Morton DC, Nagol J, Carbajal C, Rosette J, Palace M, Cook BD, Vermote EF, . . ., North PRJ (2014) Amazon forests maintain consistent canopy structure and greenness during the dry season. Nature 506:221–224

Moya I, Camenen L, Evain S, Goulas Y, Cerovic ZG, Latouche L, Flexas J (2004) A new instrument for passive remote sensing: 1. Measurement of sunlight-induced chlorophyll fluorescence. Remote Sens Environ 91:186–197

Myneni RB, Ross J (eds) (1990) Photon-vegetation Interactions: Applications in Optical Remote Sensing and Plant Ecology. Springer, Heidelberg

Myneni RB, Williams DL (1994) On the relationship between fAPAR and NDVI. Remote Sens Environ 49:200–211

Myneni RB, Ross J, Asrar G (1989) A review of the theory of photon transport in leaf canopies. Agric For Meteorol 45:1–153

Myneni RB, Asrar G, Gerstl SAW (1990) Radiative transfer in three-dimensional leaf canopies. Transp Theor Stat Phys 19:205–250

Myneni RB, Keeling CD, Tucker CJ, Asrar G, Nemani RR (1997a) Increased plant growth in the northern high latitudes from 1981 to 1991. Nature 386:698–702

Myneni RB, Nemani RR, Running SW (1997b) Estimation of global leaf area index and absorbed par using radiative transfer models. IEEE Trans Geosci Remote Sens 35:1380–1393

Myneni RB, Hofmann S, Knyazikhin Y, Privette JL, Glassy J, Tian J, Song X, . . ., Running SW (2002) Global products of vegetation leaf area and fraction absorbed PAR from year one of MODIS data. Remote Sens Environ 83:214–231

Myneni RB, Yang W, Nemani R., Huete AR, Dickinson RE, Kynazikhin Y, Didan K, . . ., Salomonson V (2007) Large seasonal swings in leaf area of Amazon rainforests. Proc Natl Acad Sci USA 104:4820–4823

Næsset E, Gobakken T, Holmgren˙ J, Hyyppä˙ H, Hyyppä˙ J, Maltamo˙ M, Nilsson M, . . ., Söderman U (2004) Laser scanning of forests: the Nordic experience. Scand J For Res 19:482–499

Nagai S, Saigusa N, Muraoka H, Nasahara KN (2010) What makes the satellite-based EVI-GPP relationship unclear in a deciduous broad-leaved forest? Ecol Res 25:359–365

Nicodemus FE, Richmond JC, Hsia JJ, Ginsberg IW, Limperis T (1977) Geometrical considerations and nomenclature for reflectance. NBS Monograph 160, National Bureau of Standards, U.S. Department of Commerce, Washington, DC

Niinemets Ü, Anten NPR (2009) Packing the photosynthetic machinery: from leaf to canopy. In: Laisk A, Nedbal L, Govindjee (eds) Photosynthesis in Silico: Understanding Complexity from Molecules to Ecosystems. Springer, Dordrecht, pp 363–399

Nilson T, Kuusk A (1989) A reflectance model for the homogenous plant canopy and its inversion. Remote Sens Environ 27:157–167

Norman JM, Miller EE, Tanner CB (1971) Light intensity and sunfleck size distribution in plant communities. Agron J 63:743–748

North PRJ (1996) Three-dimensional forest light interaction model using a Monte Carlo method. IEEE Trans Geosci Remote Sens 34:946–956

Olioso A, Méthy M, Lacaze B (1992) Simulation of canopy fluorescence as a function of canopy structure and leaf fluorescence. Remote Sens Environ 41:239–247

Olioso A, Inoue Y, Ortega-Farias S, Demarty J, Wigneron JP, Braud I (2005) Future directions for advanced evapotranspiration modeling: Assimilation of remote sensing data into crop simulation models and SVAT models. Irrig Drain Syst 19:377–412

Ollinger SV (2011) Sources of variability in canopy reflectance and the convergent properties of plants. New Phytol 189:375–394

Ollinger SV, Richardson AD, Martin ME, Hollinger DY, Frolking SE, Reich PB, Plourde LC, . . ., Schmid HP (2008) Canopy nitrogen, carbon assimilation, and albedo in temperate and boreal forests: Functional relations and potential climate feedbacks. Proc Natl Acad Sci USA 105:19336–19341

Perttunen J, Sievänen R, Nikinmaa E (1998) LIGNUM: a model combining the structure and the functioning of trees. Ecol Model 108:189–198

Pettorelli N (2013) The Normalized Difference Vegetation Index. OUP, Oxford. ISBN 978-0-19-969316-0

Pettorelli N, Vik JO, Mysterud A, Gaillard J-M, Tucker CJ, Stenseth NC (2005) Using the satellite-derived NDVI to assess ecological responses to environmental change. Trend Ecol Evol 20:503–510

Pfeifer M, Disney MI, Quaife T, Marchant R (2012) Terrestrial ecosystems from space: a review of earth observation products or macroecology applications. Glob Ecol Biogeogr 21:603–624

Pinty B, Verstraete MM, Dickinson RE (1989) A physical model for predicting bidirectional reflectances over bare soil. Remote Sens Environ 27:273–288

Pinty B, Gobron N, Widlowski J-L, Lavergne T, Verstraete MM (2004) Synergy between 1-D and 3-D radiation transfer models to retrieve vegetation canopy properties from remote sensing data. J Geophys Res 109: D21205

Pinty B, Lavergne T, Dickinson R, Widlowski J-L, Gobron N, Verstraete MM (2006) Simplifying the interaction of land surfaces with radiation for relating remote sensing products to climate models. J Geophys Res 111: D02116

Pinty B, Andredakis I, Clerici M, Kaminski T, Taberner M, Verstraete MM, Gobron N, . . ., Widlowski JL (2011a) Exploiting the MODIS albedos with the Two-stream Inversion Package (JRC-TIP). 1. Effective leaf area index, vegetation, and soil properties. J Geophys Res 116:D09105

Pinty B, Andredakis I, Clerici M, Kaminski T, Taberner M, Verstraete MM, Gobron N, . . ., Widlowski JL (2011b) Exploiting the MODIS albedos with the Two-stream Inversion Package (JRC-TIP): 2. Fractions of transmitted and absorbed fluxes in the vegetation and soil layers. J Geophys Res 116:D09106

Prusinkiewicz P, Lindenmayer A (1990) The Algorithmic Beauty of Plants. Springer, New York

Qin J, Liang S, Liu R, Zhang H, Hu B (2007) A weak-constraint-based data assimilation scheme for estimating surface turbulent fluxes. IEEE Geosci Remote Sens Lett 4:649–653

Quaife T, Lewis P, De Kauwe M, Williams M, Law BE, Disney MI (2008) Assimilating canopy reflectance data into an ecosystem model with an Ensemble Kalman Filter. Remote Sens Environ 112:1347–1364

Raumonen P, Kaasalainen M, Åkerblom M, Kaasalainen S, Kaartinen H, Vastaranta M, Holopainen M, . . ., Lewis P (2013) Comprehensive quantitative tree models from terrestrial laser scanner data. Remote Sens 5:491–520

Rautiainen M, Stenberg P (2005) Application of photon recollision probability in coniferous canopy reflectance model. Remote Sens Environ 96:98–107

Richardson AD, Anderson RS, Arain MA, Barr AG, Bohrer G, Chen G, Chen JM, . . ., Xue Y (2012) Terrestrial biosphere models need better representation of vegetation phenology: results from the North American Carbon Program Site Synthesis. Glob Chang Biol 18:566–584

Rodell M, et al (2004) Basin scale estimates of evapotranspiration using GRACE and other observations. Geophys Res Lett 31(20)

Rosema A, Verhoef W, Schroote J, Snel JFH (1991) Simulating fluorescence light-canopy interaction in support of laser-induced fluorescence measurements. Remote Sens Environ 37:117–130

Rosette JAB, North PRJ, Suarez JC (2005) Vegetation height estimates for a mixed temperate forest using

satellite laser altimetry. Int J Remote Sens 29:1475–1493
Ross JK (1981) The Radiation Regime and The Architecture of Plant Stands. Dr. W. Junk Publ, The Hague
Ross JK, Marshak AL (1989) The influence of leaf orientation and the specular component of leaf reflectance on the canopy bidirectional reflectance. Remote Sens Environ 27:251–260
Saatchi SS, Harris N, Brown S, Lefsky M, Mitchard E, Salas W, Zutta B, . . ., Morel A (2011) Benchmark map of forest carbon stocks in tropical regions across three continents. Proc Natl Acad Sci USA, 108:9899–9904
Saleska SR, Didan K, Huete AR, da Rocha HR (2007) Amazon forests green-up during 2005 drought. Science 318:612
Samanta A, Ganguly S, Hashimoto H, Devadiga S, Vermote E, Knyazikhin Y, Nemani RR, Myneni, RB (2010) Amazon forests did not green-up during the 2005 drought. Geophys Res Lett 37: L05401
Schaepman-Strub G, Schaepman ME, Painter TH, Dangel S, Martonchik JV (2006) Reflectance quantities in optical remote sensing – definitions and case studies. Remote Sens Environ 103:27–42
Schreiber U, Bilger W, Neubauer C (1995) Chlorophyll fluorescence as a nonintrusive indicator for rapid assessment of in vivo photosynthesis. In: Ecophysiology of photosynthesis. Springer, Berlin/Heidelberg, pp 49–70
Schull MA, Knayzikhin YV, Xu L, Samanta A, Carmona PL, Lepine L, Jenkins JP, . . ., Myneni RB (2011) Canopy spectral invariants, Part 2: Application to classification of forest types from hyperspectral data. J Quant Spectrosc Radiat Transf 112:736–750
Sellers PJ (1985) Canopy reflectance, photosynthesis and transpiration. Int J Remote Sens 6:1335–1372
Sitch S, Smith B, Prentice IC, Arneth A, Bondeau A, Cramer W, Kaplan JO, . . ., Venevsky S (2003) Evaluation of ecosystem dynamics, plant geography and terrestrial carbon cycling in the LPJ dynamic global vegetation model. Glob Chang Biol 9:161–185
Sivia D, Skilling J (2006) Data Analysis: A Bayesian Tutorial, 2nd edn. Oxford University Press, Oxford
Smolander S, Stenberg P (2005) Simple parameterizations of the radiation budget of uniform broadleaved and coniferous canopies. Remote Sens Environ 94:355–363
Solomon SD, Qin M, Manning M, Chen M, Marquis MB, Averyt M, Tignor M, Miller HL (eds) (2007) Contribution of Working Group I to the Fourth Assessment Report of the Intergovernmental Panel on Climate Change, 2007
Strahler AH (1996) Vegetation canopy reflectance modeling: recent developments and remote sensing perspectives. Remote Sens Rev 15:179–194
Suits GH (1972) The calculation of the directional reflectance of a vegetative canopy. Remote Sens Environ 2:117–125
Tang H, Dubayah R, Swatantran A, Hofton M, Sheldon S, Clark D, Blair B (2012) Retrieval of vertical LAI profiles over tropical rain forests using waveform lidar at La Selva, Costa Rica. Remote Sens Environ 124:242–250
Tarantola A (2005) Inverse Problem Theory and Methods for Model Parameter Estimation, Society for the Industrial and Applied Mathematics (SIAM), Philadelphia, PA
Twomey S (1977) Introduction to the Mathematics of Inversion in Remote Sensing and Indirect Measurements. Elsevier, Amsterdam
Ustin S (2013) Remote sensing of canopy chemistry. Proc Natl Acad Sci USA 110: 804–805
Vargas I, Niklasson GA (1997) Applicability conditions of the Kubelka-Munk theory. Appl Opt 36:5580–5586
Verhoef W (1984) Light-scattering by leaf layers with application to canopy reflectance modeling – the SAIL model. Remote Sens Environ 16:125–141
Verstraete, MM, Pinty B, Dickinson RE (1990) A physical model of the bidirectional reflectance of vegetation canopies. 1. Theory. J Geophys Res 95. D8:11
Verstraete MM, Pinty B, Myneni RB (1996) Potential and limitations for information extraction from remote sensing. Remote Sens Environ 58:201–214
Wang WM, Li ZL, Su HB (2007) Comparison of leaf angle distribution functions: effects on extinction coefficient and fraction of sunlit foliage. Agric For Meteorol 143:106–122
Wanner W, Strahler AH, Hu B, Lewis P, Muller JP, Li X, Barker-Schaaf CL, Barnsley MJ (1997) Global retrieval of bidirectional reflectance and albedo over land from EOS MODIS and MISR data: theory and algorithm. J Geophys Res 102:17143–17161
Widlowski JL, Lavergne T, Pinty B, Verstraete MM, Gobron N (2006) Rayspread: A virtual laboratory for rapid BRF simulations over 3-D plant canopies. In: Frank G (ed) Computational Methods in Transport, Lecture Notes in Computational Science and Engineering Series, 48. Springer, Berlin, pp 211–231
Widlowski JL, Taberner M, Pinty B, Bruniquel-Pinel V, Disney MI, Fernandes R, Gastellu-Etchegorry JP, . . ., Xie D (2007) The third Radiation transfer Model Intercomparison (RAMI) exercise: Documenting progress in canopy reflectance modelling, J Geophys Res 112: D09111

Widlowski JL, Robustelli M, Disney MI, Gastellu-Etchegorry JP, Lavergne T, Lewis P, North PRJ, . . ., Verstraete MM (2008) The RAMI On-line Model Checker (ROMC): A web-based benchmarking facility for canopy reflectance models. Remote Sens Environ 112:1144–1150

Widlowski JL, Pinty B, Clerici M, Dai Y., De Kauwe M, de Ridder K, Kallel A, . . ., Yuan H (2011) RAMI4PILPS: An intercomparison of formulations for the partitioning of solar radiation in land surface models. J Geophys Res 116: G02019, 25

Widlowski JL, Pinty B, Lopatka M, Aztberger C, Buzica D, Chelle M, Disney MI, . . ., Xie D (2013) The fourth Radiation transfer Model Intercomparison (RAMI-IV): Proficiency testing of canopy reflectance models with ISO-13528, J Geophys Res 118:1–22

Woodhouse IH, Nichol C, Sinclair P, Jack J, Morsdorf F, Malthus TJ, Patenaude G (2011) A multispectral canopy LiDAR demonstrator project. IEEE Geosci Remote Sens Lett 8:839–843

Woodhouse IH, Mitchard ETA, Brolly M, Maniatis D, Ryan CM (2012) Radar backscatter is not a 'direct measure' of forest biomass. Nat Clim Change 2:556–557

Wulder M, White J, Nelson R, Næsset E, Ørka H, Coops N, Hilker T, . . ., Gobakken T (2012) Lidar sampling for large-area forest characterization: A review. Remote Sens Environ 121:196–209

Yao T, Yang X, Zhao F, Wang Z, Zhang Q, Jupp D, Lovell J, . . ., Strahler A (2011) Measuring forest structure and biomass in New England forest stands using Echidna ground-based lidar. Remote Sens Environ 115:1144–1150

Zarco-Tejada P, Miller JR, Pedros R, Verhoef W, Berger M (2006) FluorMODgui V3.0: a graphic user interface for the spectral simulation of leaf and canopy chlorophyll fluorescence. Comput Geosci 32:577–591

Zarco-Tejada PJ, Bernia JAJ, Suárez L, Sepulcre-Cantó G, Morales F, Miller JR (2009) Imaging chlorophyll fluorescence with an airborne narrow-band multispectral camera for vegetation stress detection. Remote Sens Environ 113:1262–1275